Inorg. Chem. **2008**, *47*, 11470−11486

The Contrasting Chemistry and Cancer Cell Cytotoxicity of Bipyridine and Bipyridinediol Ruthenium(II) Arene Complexes

Tijana Bugarcic,[†,‡] Abraha Habtemariam,[‡] Jana Stepankova,[||] Pavla Heringova,[||] Jana Kasparkova,[||,§] Robert J. Deeth,[‡] Russell D. L. Johnstone,[†] Alessandro Prescimone,[†] Andrew Parkin,[†] Simon Parsons,[†] Viktor Brabec,[||] and Peter J. Sadler[‡,*]

School of Chemistry, University of Edinburgh, West Mains Road, Edinburgh EH9 3JJ, U.K., Department of Chemistry, University of Warwick, Coventry C4V 7AL, U.K., Institute of Biophysics, Academy of Sciences of the Czech Republic, v.v.i., Kralovopolska 135, CZ-61265 Brno, Czech Republic, and Laboratory of Biophysics, Department of Experimental Physics, Faculty of Sciences, Palacky University, tr. Svobody 26, CZ-77146 Olomouc, Czech Republic

Received July 21, 2008

The synthesis and characterization of ruthenium(II) arene complexes $[(\eta^6\text{-arene})Ru(N,N)Cl]^{0/+}$, where N,N = 2,2′-bipyridine (bipy), 2,2′-bipyridine-3,3′-diol (bipy$(OH)_2$) or deprotonated 2,2′-bipyridine-3,3′-diol (bipy(OH)O) as N,N-chelating ligand, arene = benzene (bz), indan (ind), biphenyl (bip), *p*-terphenyl (*p*-terp), tetrahydronaphthalene (thn), tetrahydroanthracene (tha) or dihydroanthracene (dha), are reported, including the X-ray crystal structures of $[(\eta^6\text{-tha})Ru(bipy)Cl][PF_6]$ (**1**), $[(\eta^6\text{-tha})Ru(bipy(OH)O)Cl]$ (**2**) and $[(\eta^6\text{-ind})Ru(bipy(OH)_2)Cl][PF_6]$ (**8**). Complexes **1** and **2** exibit CH (arene)/π (bipy or bipy(OH)O) interactions. In the X-ray structure of protonated complex **8**, the pyridine rings are twisted (by 17.31°). In aqueous solution (pH = 2−10), only deprotonated (bipy(OH)O) forms are present. Hydrolysis of the complexes was relatively fast in aqueous solution ($t_{1/2}$ = 4−15 min, 310 K). When the arene is biphenyl, initial aquation of the complexes is followed by partial arene loss. Complexes with arene = tha, thn, dha, ind and *p*-terp, and deprotonated bipyridinediol (bipy(OH)O) as chelating ligands, exhibited significant cytotoxicity toward A2780 human ovarian and A549 human lung cancer cells. Complexes $[(\eta^6\text{-bip})Ru(bipy(OH)O)Cl]$ (**7**) and $[(\eta^6\text{-bz})Ru(bipy(OH)O)Cl]$ (**5**) exhibited moderate cytotoxicity toward A2780 cells, but were inactive toward A549 cells. These activity data can be contrasted with those of the parent bipyridine complex $[(\eta^6\text{-tha})Ru(bipy)Cl][PF_6]$ (**1**) which is inactive toward both A2780 ovarian and A549 lung cell lines. DFT calculations suggested that hydroxylation and methylation of the bipy ligand have little effect on the charge on Ru. The active complex $[(\eta^6\text{-tha})Ru(bipy(OH)O)Cl]$ (**2**) binds strongly to 9-ethyl-guanine (9-EtG). The X-ray crystal structure of the adduct $[(\eta^6\text{-tha})Ru(bipy(OH)O)(9\text{-EtG-}N7)][PF_6]$ shows intramolecular CH (arene)/π (bipy(OH)O) interactions and DFT calculations suggested that these are more stable than arene/9-EtG $\pi-\pi$ interactions. However $[(\eta^6\text{-ind})Ru(bipy(OH)_2)Cl][PF_6]$ (**8**) and $[(\eta^6\text{-ind})Ru(bipy)Cl][PF_6]$ (**16**) bind only weakly to DNA. DNA may therefore not be the major target for complexes studied here.

Introduction

Metal complexes offer potential in medicinal chemistry and drug design;[1,2] in particular, ruthenium complexes are attracting current interest.[3−5] Organoruthenium complexes of the type $[(\eta^6\text{-arene})Ru^{II}(YZ)X]^+$, where the arene is benzene or a benzene derivative, YZ is a chelating ligand and X is a halide, have been studied as potential anticancer agents.[6−8] Complexes containing chelating ligands tend to be more active than those containing only monodentate ligands.[6] Ruthenium(II) arene complexes in which the

* To whom correspondence should be addressed. E-mail: P.J.Sadler@warwick.ac.uk.
† School of Chemistry, University of Edinburgh.
‡ Department of Chemistry, University of Warwick.
|| Institute of Biophysics.
§ Palacky University.

(1) Berners-Price, S. J.; Sadler, P. J. *Coord. Chem. Rev.* **1996**, *151*, 1–40.
(2) Guo, Z.; Sadler, P. J. *Angew. Chem., Int. Ed.* **1999**, *38*, 1512–1531.
(3) Clarke, M. J. *Coord. Chem. Rev.* **2003**, *236*, 209–233.
(4) Dougan, S. J.; Sadler, P. J. *Chimia* **2007**, *61*, 704–715.
(5) Ang, W. H.; Dyson, P. J. *Eur. J. Inorg. Chem.* **2006**, 4003–4018.

10.1021/ic801361m CCC: $40.75
Published on Web 11/14/2008

chelating ligand is ethylenediamine (en) and the leaving group is Cl^- are cytotoxic to cancer cells, including cell lines that are resistant to cisplatin.[6,7] Hydrolysis of the ruthenium−chloride bond is thought to generate a reactive site for potential DNA binding.[9] In this class of complexes, the arene provides a hydrophobic face for the complex and stabilizes ruthenium in the +2 oxidation state so that oxidation to Ru^{III} is difficult. Cytotoxicity increases with the size of the arene.[6] The chelating ligand provides additional stability.

Recently, we reported structure−activity relationships for Ru^{II} arene complexes containing N, N-chelating ligands.[10] It was notable that although complexes containing en as chelating ligand were active (cytotoxic to cancer cells), complexes containing tetramethyl-en or bipyridine as chelating ligands were inactive, suggesting that NH groups on the chelating ligand play a role in the activity, perhaps stabilizing guanine adducts on DNA via H-bonding. Indeed, stereospecific H-bonding has been observed between ethylenediamine (en) NH···C6O of 9-ethylguanine (9-EtG) in the crystal structures of $[(\eta^6\text{-tha})Ru^{II}(en)(9\text{-EtG})]^{2+}$ and $[(\eta^6\text{-dha})Ru^{II}(en)(9\text{-EtG})]^{2+}$ (distances of 1.9 and 2.1 Å, respectively).[11]

In the present work, we have discovered that the presence of hydroxyl groups at the 3,3′-positions of 2,2′-bipyridine (2,2′-bipyridine-3,3′-diol) dramatically alters the activity profile of these Ru^{II} arene complexes. Unlike en, which is purely a σ-donor, the bipyridine derivatives are σ-donors and π-acceptors, and as π-acceptors make the metal center more acidic. The 3,3′-positions in 2,2′-bipyridine are different from the other positions on the ligand; for example, they have been reported to introduce steric strain upon the 3,3′-protons in $[Ru(bipy)_3]^{2+}$.[12] When 2,2′-bipyridine-3,3′-diol chelates to a metal, steric constraint is introduced[13] by the proximity of the two hydroxyl substituents and the strain is released upon the formation of an O−H···O H-bond with deprotonation of one of the OH groups.

It was of interest, therefore, in the present work, to compare the aqueous solution chemistry, solid-state structures and cytotoxicity of Ru^{II} arene complexes containing bipyridine (bipy), bipyridinediol ($bipy(OH)_2$) or deprotonated bipyridinediol (bipy(OH)O) as N,N-chelating ligands. Eight chlorido Ru^{II} arene complexes containing bipy, $bipy(OH)_2$ or bipy(OH)O with a variety of arenes were synthesized and the structures of complexes $[(\eta^6\text{-tha})Ru(bipy)Cl][PF_6]$ (**1**), $[(\eta^6\text{-tha})Ru(bipy(OH)O)Cl]$ (**2**) and $[(\eta^6\text{-ind})Ru(bipy(OH)_2)Cl][PF_6]$ (**8**) were determined by X-ray crystallography. The effects of hydroxylation and methylation of the bipy ligand on the electron distribution were studied using DFT calculations. The aqueous solution chemistry of these complexes (hydrolysis, arene loss and acidity of OH protons of bound $bipy(OH)_2$ and bipy(OH)O) has been investigated, as well as interactions with the DNA model nucleobase 9-ethylguanine (9-EtG) both in solution and by X-ray crystallography, and cytotoxicity toward human ovarian (A2780) and human lung (A549) cancer cells. In addition, DNA binding studies were performed with complexes $[(\eta^6\text{-ind})Ru(bipy(OH)_2)Cl][PF_6]$ (**8**) and $[(\eta^6\text{-ind})Ru(bipy)Cl][PF_6]$ (**16**).

Experimental Section

Materials. The starting materials $[(\eta^6\text{-arene})RuCl_2]_2$, arene = benzene (bz), indan (ind), biphenyl (bip), *p*-terphenyl (*p*-terp, bound to Ru through the terminal phenyl ring), tetrahydronaphthalene (thn), tetrahydroanthracene (tha), or dihydroanthracene (dha), were prepared according to literature methods.[14,15] 2,2′-Bipyridine-3,3′-diol, 2,2′-bipyridine, *N*-methylimidazole (N-MeIm) and 9-ethylguanine (9-EtG) were purchased from Sigma-Aldrich. Ethanol and methanol were dried over Mg/I_2. Complexes $[(\eta^6\text{-ind})Ru(4,4'\text{-}Me_2\text{-bipy-})Cl][PF_6]$ (**13**), $[(\eta^6\text{-ind})Ru(phen)Cl][PF_6]$ (**14**), $[(\eta^6\text{-bip})Ru(bipy-)Cl][PF_6]$ (**15**) and $[(\eta^6\text{-ind})Ru(bipy)Cl][PF_6]$ (**16**) were prepared as previously described.[10] Cisplatin was obtained from Sigma-Aldrich sro (Prague, Czech Republic). Chloridodiethylenetriamine-platinum(II) chloride ([PtCl(dien)]Cl) was a generous gift of Professor G. Natile from University of Bari. Stock aqueous solutions of metal complexes (5×10^{-4} M) for the biophysical and biochemical studies were filtered and stored at room temperature in the dark. The concentrations of ruthenium or platinum in the stock solutions were determined by flameless atomic absorption spectrometry (FAAS). Calf thymus (CT) DNA (42% G + C, mean molecular mass ca. 2×10^7) was also prepared and characterized as described previously.[16,17] pSP73KB (2455 bp) plasmid was isolated according to standard procedures. Restriction endonucleases *Nde*I and T4 polynucleotide kinase were purchased from New England Biolabs. Sequenase 2 was from USB Corporation (Cleveland, OH). Acrylamide, bis(acrylamide) and ethidium bromide (EtBr) were obtained from Merck KgaA (Darmstadt, Germany). Agarose was purchased from FMC BioProducts (Rockland, ME). Radioactive products were obtained from MP Biomedicals, LLC (Irvine, CA).

Synthesis of Ruthenium Complexes. All compounds were synthesized in methanol using a similar procedure. Typically, the ligand (2 mol equiv) was added to a methanolic solution of the ruthenium dimer $[(\eta^6\text{-arene})RuCl_2]_2$. Details for individual reactions are described below.

$[(\eta^6\text{-Tha})Ru(bipy)Cl][PF_6]$ (1). To a suspension of $[(\eta^6\text{-tha})RuCl_2]_2$ (0.053 g, 0.075 mmol) in dry, freshly distilled methanol (25 mL) was added bipyridine (0.023 g, 0.150 mmol). The reaction mixture was stirred at ambient temperature under argon, overnight. The resulting clear yellow solution was filtered, NH_4PF_6 (0.060 g, 0.374 mmol) was added and the flask was shaken. A precipitate

(6) Aird, R. E.; Cummings, J.; Ritchie, A. A.; Muir, M.; Morris, R. E.; Chen, H.; Sadler, P. J.; Jodrell, D. I *Br. J. Cancer* **2002**, *86*, 1652–1657.
(7) Morris, R. E.; Aird, R. E.; Murdoch, P. d. S.; Chen, H.; Cummings, J.; Hughes, N. D.; Parsons, S.; Parkin, A.; Boyd, G.; Jodrell, D. I.; Sadler, P. J *J. Med. Chem.* **2001**, *44*, 3616–3621.
(8) Yan, Y. K.; Melchart, M.; Habtemariam, A.; Sadler, P. J. *Chem. Comm.* **2005**, 4764–4776.
(9) Chen, H.; Parkinson, J. A.; Morris, R. E.; Sadler, P. J. *J. Am. Chem. Soc.* **2003**, *125*, 173–186.
(10) Habtemariam, A.; Melchart, M.; Fernandez, R.; Parsons, S.; Oswald, I. D. H.; Parkin, A.; Fabbiani, F. P. A.; Davidson, J. E.; Dawson, A.; Aird, R. E.; Jodrell, D. I.; Sadler, P. J. *J. Med. Chem.* **2006**, *49*, 6858–6868.
(11) Chen, H.; Parkinson, J. A.; Parsons, S.; Coxall, R. A.; Gould, R. O.; Sadler, P. J. *J. Am. Chem. Soc.* **2002**, *124*, 3064–3082.
(12) Constable, E. C.; Seddon, K. R. *J. Chem. Soc., Chem. Commun.* **1982**, 34–36.
(13) Thompson, A. M. W. C.; Jeffery, J. C.; Liard, D. J.; Ward, M. D. *J. Chem. Soc., Dalton Trans.* **1996**, 879–884.
(14) Zelonka, R. A.; Baird, M. C *Can. J. Chem.* **1972**, *50*, 3063–3072.
(15) Beasley, T. J.; Brost, R. D.; Chu, C. K.; Grundy, S. L.; Stobart, S. R. *Organometallics* **1993**, *12*, 4599–4606.
(16) Brabec, V.; Palecek, E. *Biophys. Chem.* **1976**, *4*, 79–92.
(17) Brabec, V.; Palecek, E. *Biophysik (Berlin)* **1970**, *6*, 290–300.

started to appear almost immediately. The flask was kept at 253 K overnight, and the product was collected by filtration, washed with cold methanol and ether, and dried in air to give a brownish solid.

Yield: 0.036 g (39%). Crystals suitable for X-ray analysis were obtained by slow evaporation of a methanolic solution at ambient temperature and the complex crystallized as [(η^6-tha)Ru(bipy)Cl]-[PF_6]·H_2O. ^{1}H NMR in DMSO-d_6: δ 9.55 (d, 2H), 8.6 (d, 2H), 8.3 (dd, 2H), 7.85 (m, 2H), 6.4 (dd, 2H), 6.1 (dd, 2H), 5.45 (s, 2H), 3.12 (m, 2H), 2.43 (m, 4H), 1.5 (m, 2H). Anal. Calcd for $C_{24}H_{24}ClF_6N_2PORu$ (**1**·H_2O): C, 45.33; H, 3.80; N, 4.41. Found: C, 45.43; H, 3.40; N, 4.55.

[(η^6-Tha)Ru(bipy(OH)O)Cl] (2). To a suspension of [(η^6-tha)$RuCl_2$]$_2$ (0.050 g, 0.070 mmol) in dry, freshly distilled methanol (25 mL), 2,2′-bipyridine-3,3′-diol (0.026 g, 0.140 mmol) was added. The reaction mixture was stirred at ambient temperature under argon overnight, filtered and the volume was reduced until the onset of precipitation. It was kept at 277 K for 24 h to allow further precipitation to occur. The fine yellow solid was collected by filtration, washed with methanol followed by ether, and dried in vacuum. It was recrystallized from methanol/ether.

Yield: 0.036 g (51.0%). A portion of the complex (1 mg) was dissolved in methanol (1 mL) and filtered to yield a clear yellow solution. Slow diffusion of diethyl ether into this solution resulted in the formation of yellow crystals suitable for X- ray diffraction. ESI-MS: calcd for $C_{24}H_{22}ClN_2O_2Ru^+$ [M + H]$^+$ *m*/*z* 507.0, found 507.3. ^{1}H NMR in DMSO-d_6: δ 17.92 (s, 1H, OH), 8.62 (d, 2H), 7.22 (dd, 2H), 7.06 (d, 2H), 6.08 (dd, 2H), 5.91 (dd, 2H), 5.56 (s, 2H), 3.12 (m, 2H), 2.43 (m, 4H), 1.92 (m, 2H).

[(η^6-Dha)Ru(bipy(OH)O)Cl] (3). To a suspension of [(η^6-dha)$RuCl_2$]$_2$ (0.028 g, 0.040 mmol) in dry, freshly distilled methanol (30 mL), 2,2′-bipyridine-3,3′-diol (0.015 g, 0.080 mmol) was added. The rest of the procedure was the same as described for **2**. The fine yellow solid was recrystallized from methanol/ether.

Yield: 0.016 g (41.0%). ESI-MS: calcd for $C_{24}H_{20}ClN_2O_2Ru^+$ [M + H]$^+$ *m*/*z* 504.9, found 504.8. ^{1}H NMR in MeOD-d_4: δ 17.69 (s, 1H, OH), 8.62 (d, 2H), 7.14 (dd, 2H), 6.95 (d, 2H), 6.89 (d, 2H), 6.63 (t, 2H), 6.30 (d, 2H), 5.96 (t, 2H), 4.17 (d, 2H), 3.77 (d, 2 H).

[(η^6-Thn)Ru(bipy(OH)O)Cl] (4). To a suspension of [(η^6-thn)$RuCl_2$]$_2$ (0.030 g, 0.050 mmol) in dry, freshly distilled methanol (30 mL), 2,2′-bipyridine-3,3′-diol (0.018 g, 0.100 mmol) was added. The rest of the procedure was the same as described for **2**, the only difference was that the reaction mixture was stirred for 4 h instead of overnight. The fine yellow solid was recrystallized from methanol/ether.

Yield: 0.030 g (67.8%). ESI-MS: calcd for $C_{20}H_{20}ClN_2O_2Ru^+$ [M + H]$^+$ *m*/*z* 456.9, found 457.3. ^{1}H NMR in DMSO-d_6: δ 17.92 (s, 1H, OH), 8.66 (d, 2H), 7.27 (dd, 2H), 7.10 (d, 2H), 5.96 (t, 2H), 5.84 (d, 2H), 2.54 (m, 2H), 2.20 (m, 2H), 1.52 (m, 2H), 1.20 (m, 2H).

[(η^6-Bz)Ru(bipy(OH)O)Cl] (5). To a suspension of [(η^6-bz)$RuCl_2$]$_2$ (0.052 g, 0.106 mmol) in dry, freshly distilled methanol (30 mL), 2,2′-bipyridine-3,3′-diol (0.040 g, 0.213 mmol) was added. The rest of the procedure was the same as described for **2**, the only difference was that the reaction mixture was stirred for 3 h instead of overnight. The fine yellow solid was recrystallized from methanol/ether.

Yield: 0.060 g (72.0%). ^{1}H NMR in DMSO-d_6: δ 17.89 (s, 1H, OH), 8.78 (d, 2H), 7.21 (dd, 2H), 7.09 (d, 2H), 6.05 (s, 6H). Anal. Calcd for $C_{16}H_{13}ClN_2O_2Ru$·$0.5H_2O$ (**5**·$0.5H_2O$): C, 46.77; H, 3.43; N, 6.82. Found: C, 46.72; H, 2.83; N, 6.68.

[(η^6-*p*-Terp)Ru(bipy(OH)O)Cl] (6). To a suspension of [(η^6-*p*-terp)$RuCl_2$]$_2$ (0.050 g, 0.062 mmol) in dry, freshly distilled methanol (50 mL), 2,2′-bipyridine-3,3′-diol (0.023 g, 0.124 mmol) was added. The rest of the procedure was the same as described for **2**. The fine yellow solid was recrystallized from acetone/ether.

Yield: 0.051 g (74.6%). ^{1}H NMR in DMSO-d_6: δ 17.91 (s, 1H, OH), 8.5 (d, 2H), 7.75 (m, 6H), 7.5 (t, 2H), 7.4 (t, 1H), 7.1 (m, 4H), 6.5 (d, 2H), 6.2 (t, 2H), 6.1 (t, 1H). Anal. Calcd for $C_{28}H_{23}ClN_2O_3Ru$ (**6**·H_2O): C, 58.79; H, 4.05; N, 4.89. Found: C, 59.22; H, 3.41; N, 4.69.

[(η^6-Bip)Ru(bipy(OH)O)Cl] (7). To a suspension of [(η^6-bip)$RuCl_2$]$_2$ (0.053 g, 0.08 mmol) in dry, freshly distilled methanol (30 mL), 2,2′-bipyridine-3,3′-diol (0.030 g, 0.16 mmol) was added. The rest of the procedure was the same as described for **2**. The fine yellow solid was recrystallized from acetone/ether.

Yield: 0.049 g (63.0%). ^{1}H NMR in DMSO-d_6: δ 17.85 (s, 1H, OH), 8.5 (d, 2H), 7.7 (t, 1H), 7.6 (d, 2H), 7.4 (t, 2H), 7.00 (m, 4H), 6.5 (d, 2H), 6.2 (t, 2H), 6.1 (t, 1H). Anal. Calcd for $C_{22}H_{17}ClN_2O_2Ru$: C, 55.29; H, 3.58; N, 5.86. Found: C, 55.36; H, 3.27; N, 5.88.

[(η^6-Ind)Ru(bipy(OH$_2$)Cl][PF_6] (8). To a suspension of [(η^6-ind)$RuCl_2$]$_2$ (0.075 g, 0.13 mmol) in dry, freshly distilled methanol (10 mL), 2,2′-bipyridine-3,3′-diol (0.050 g, 0.26 mmol) dissolved in methanol (3 mL) was added dropwise. The reaction mixture was left stirring at ambient temperature for 1 h. It was then filtered, and to the filtrate, NH_4PF_6 (0.128 g, 0.80 mmol) was added and the flask shaken. A precipitate started to appear almost immediately. The flask was kept at 253 K overnight. The solid obtained was collected by filtration, washed with cold methanol and ether and dried in air to give an intense bright yellow solid.

Yield: 0.079 g (52%). Crystals suitable for X-ray analysis were obtained by slow evaporation of a methanolic solution at ambient temperature as [(η^6-ind)Ru(bipy(OH$_2$)Cl][PF_6]·CH_3OH. ^{1}H NMR in DMSO-d_6 δ: 8.60 (d, 2H), 7.27 (dd, 2H), 7.05 (d, 2H), 6.10 (m, 2H), 5.82 (m, 2H), 2.67−2.50, 2.05−1.85 (m, 6H), Anal. Calcd for $C_{19}H_{18}ClF_6N_2O_2PRu$: C, 39.73; H, 3.67; N, 4.63. Found: C, 39.03; H, 3.66; N, 4.66.

[(η^6-Tha)Ru(bipy)(9-EtG-*N7*)][PF_6]$_2$ (9). To a suspension of [(η^6-tha)Ru(bipy)Cl][PF_6] (0.020 g, 0.030 mmol) in water (30 mL), 9-ethylguanine (0.006 g, 0.030 mmol) was added. The reaction mixture was left stirring for 2 h at 310 K. The clear yellow solution was then filtered and to the filtrate NH_4PF_6 (0.026 g, 0.160 mmol) was added. The volume was reduced until the onset of precipitation. The flask was sealed and placed on ice for 2 h for further precipitation to occur. The precipitate was filtered off, washed with water followed by ethanol and ether, and dried in vacuum to give a brown solid.

ESI-MS: calcd for $C_{31}H_{31}N_7ORu^+$ [M- H]$^+$ *m*/*z* 618.7, found 619.0. ^{1}H NMR in DMSO-d_6 (90% of complex **9**): δ 11.1 (broad, 1H, NH), 10.0 (d, 2H), 8.6 (d, 2H), 8.3 (dd, 2H), 7.9 (m, 2H), 7.4 (s, 1H), 7.0 (broad, 2H, NH), 6.65 (dd, 2H), 6.10 (dd, 2H), 5.4 (s, 2H), 3.8 (q, 2H), 3.18 (d, 2H), 2.30 (m, 4H), 1.3 (d, 2H), 1.15 (t, 3H).

[(η^6-Tha)Ru(bipy(OH)O)(9-EtG-*N7*)][PF_6] (10). To a suspension of [(η^6-tha)Ru(bipy(OH)O)Cl] (0.020 g, 0.030 mmol) in water (30 mL), 9-ethylguanine (0.006 g, 0.030 mmol) was added. The reaction mixture was left stirring for 2 h at 310 K. The clear yellow solution was filtered, and to the filtrate, NH_4PF_6 (0.020 g, 0.150 mmol) was added. The rest of the procedure was the same as for **9**. The complex (1 mg) was dissolved in methanol (1 mL) and filtered to yield a clear yellow solution. Slow diffusion of diethyl ether into this solution resulted in the formation of brown crystals suitable for X-ray diffraction.

ESI-MS: calcd for $C_{31}H_{30}N_7O_3Ru^+$ $[M]^+$ *m/z* 649.7, found 650.0. ^{1}H NMR in MeOD-d_4 (98% of complex **10**): δ 17.88 (s, 1H, OH), 9.14 (d, 2H), 7.39 (dd, 2H), 7.26 (d, 2H), 7.12 (s, 1H), 6.25 (dd, 2H), 6.00 (dd, 2H), 5.53 (s, 2H), 3.95 (q, 2H), 3.18 (d, 2H), 2.45 (m, 4H), 1.79 (d, 2H), 1.25 (t, 3H).

[(η^6-Thn)Ru(bipy(OH)O)(N-MeIm)][PF_6] (11). To a suspension of [(η^6-thn)Ru(bipy(OH)O)Cl] (0.014 g, 0.023 mmol) in water (30 mL), $AgNO_3$ (0.0039 g, 0.023 mmol) was added. The reaction mixture was left stirring overnight at ambient temperature covered with aluminum foil. It was then filtered to remove AgCl, and to the filtrate, *N*-methylimidazole (1.85 μL, 0.023 mmol) in methanol (5 mL) was added. The reaction mixture was left stirring for 3 h at 310 K. The clear yellow solution was then filtered and the volume reduced to ~5 mL. NH_4PF_6 was added (0.058 g, 0.35 mmol) and the flask sealed and placed on ice for 2 h for further precipitation to occur. The yellow precipitate was filtered off, washed with a little water followed by ethanol and ether, and dried in vacuum. It was recrystallized from methanol.

Yield: 0.013 g (66.7%). The complex (1 mg) was dissolved in methanol (1 mL) and filtered to yield a clear yellow solution. Slow evaporation of this solution resulted in the formation of yellow crystals suitable for X-ray diffraction. ^{1}H NMR in DMSO δ: 17.88 (s, 1H, OH), 8.82 (d, 2H), 7.70 (s, 1H), 7.39 (t, 2H), 7.21 (d, 2H), 6.65 (dd, 2H), 6.19 (t, 2H), 6.00 (d, 2H), 3.65 (s, 3H), 2.67 (m, 2H), 2.06 (m, 2H), 1.60 (m, 2H), 1.16 (m, 2H).

[(η^6-Bz)Ru(bipy(OH)O)(9-EtG-*N7*)][PF_6] (12). To a suspension of [(η^6-bz)Ru(bipy(OH)O)Cl] (0.030 g, 0.060 mmol) in water (30 mL), 9-ethylguanine (0.011 g, 0.06 mmol) was added. The reaction mixture was left stirring for 2 h at 310 K. The clear yellow solution was filtered, and to the filtrate, NH_4PF_6 (0.029 g, 0.180 mmol) was added. The rest of the procedure was the same as for **9**. It was recrystallized from methanol to give bright yellow solid.

ESI-MS: calcd for $C_{23}H_{22}N_7O_3Ru^+$ $[M]^+$ *m/z* 545.6, found 545.9. ^{1}H NMR in DMSO-d_6 (100% of complex **12**): δ 17.6 (s, 1H, OH), 11.0 (broad, 1H, NH), 9.1 (d, 2H), 7.35 (dd, 2H), 7.15 (d, 2H), 7.05 (s, 1H), 6.9 (broad, 2H, NH), 6.2 (s, 6H), 4.0 (dd, 2H), 1.2 (t, 3H).

X-ray Crystallography. All diffraction data were collected with Mo Kα radiation on a Bruker SMART APEX CCD diffractometer equipped with an Oxford Cryosystems low-temperature device operating at 150 K. Absorption corrections were applied using the multiscan procedure SADABS.[18] Structures **1** and **10** were solved by direct methods (SIR92)[19] and refined using CRYSTALS;[20] **2**, **8** and **11** were solved using Patterson methods (SHELXS-97[21] or DIRDIF)[22] and refined with SHELXL-97.[23] In most cases, H atoms were placed in idealized positions. In complex **1**, H-atoms belonging to the water of crystallization were located in a difference map and the positions refined subject to the restraint that the OH distance was equal to 0.85(1) Å. In complex **2**, H52 was located in a difference map in a bridging position between O52 and O82; it was refined freely with an isotropic displacement parameter. H-atoms in complex **8** attached to methyl and hydroxyl groups were located in a difference synthesis and refined using the Sheldrick rigid rotating group model. In complex **10**, the H-atoms were located in a difference map, idealized, and then allowed to ride on their parent atoms; H231 is involved in an hydrogen bond, and its position was refined freely. In complex **11**, the thn ligand is disordered at C81 over two positions in the ratio 0.85:0.15. Similarity restraints were applied to the geometry about the part-weight atoms. Only the major component (C81) was refined with anisotropic displacement parameters. The expected formula for a protonated bipy(OH)$_2$ chelating ligand had 2 PF_6^- per formula unit, but only one was located in the crystal structure. A difference map in the region of the two O-atoms attached to the bipy showed one peak in a bridging position between the two O-atoms, bonded predominantly to O52. This was interpreted as a bridging O···H···O H-bond, with the overall charge on the ligand being −1, thus, ensuring change balance. The hydroxyl group O52−H52 was treated as a variable metric rigid group. The crystal structures of **1**, **2**, **8**, **10** and **11** have been deposited in the Cambridge Crystallographic Data Center under the accession numbers CCDC 676256, 676253, 611053, 676255 and 676254, respectively.

NMR Spectroscopy. All NMR spectra were recorded on either Bruker DPX (^{1}H 360 MHz), DMX (500 MHz) or AVA (600 MHz) spectrometers. ^{1}H NMR signals were referenced to the residual solvent peak, δ 2.52 (DMSO) and δ 3.34 (methanol). pH titrations were recorded on the Bruker DMX 500 spectrometer, with dioxan as an internal reference (δ 3.75). All spectra were recorded at 298 K unless stated otherwise, using 5 mm diameter tubes. The data were processed using XWIN-NMR (Version 3.6 Bruker UK Ltd.).

Elemental Analysis. Elemental analyses were carried out by the University of Edinburgh using an Exeter analytical analyzer CE440 or by the University of St. Andrews using a Carlo Erba CHNS analyzer.

Electrospray Mass Spectrometry. ESI-MS were obtained on a Micromass Platform II mass spectrometer and solutions were infused directly. The capillary voltage was 3.5 V and the cone voltage was either 15 or 25 V, depending on the solution. The source temperature was 353 K.

UV−Vis Spectroscopy. A Perkin-Elmer Lambda-16 UV−vis spectrophotometer was used with quartz cuvettes (1 cm path length; 0.5 mL) and PTP1 Peltier temperature controller. Experiments were carried out at 310 K unless otherwise stated.

pH Measurement. The pH values of NMR samples in D_2O were measured at 298 K directly in the NMR tube before and after recording NMR spectra using a Corning pH meter 145 calibrated with pH 4, pH 7 and pH 10 buffer solutions (Sigma Aldrich) and equipped with an Aldrich microcombination electrode. No corrections have been made for the effect of deuterium on the glass electrode and these are termed as pH* values. The pH* values were adjusted with NaOD and DCl of varying concentrations.

Hydrolysis. Hydrolysis of chlorido complexes was monitored by UV-vis spectroscopy or by ^{1}H NMR spectroscopy. For UV-vis spectroscopy, complexes were dissolved in methanol and diluted with H_2O to give ca. 50 μM solutions (95% H_2O, 5% MeOH). The absorbance was recorded at 30 or 60 s intervals at the selected wavelength over ca. 4 h at 310 K. Plots of the change in absorbance with time were fitted to the appropriate equation for pseudo first-order kinetics using Origin version 7.5 (Microcal Software Ltd.) to give the half-lives and rate constants. For ^{1}H NMR spectroscopy, complexes were dissolved in MeOD-d_4 and diluted in D_2O to give ca. 100 μM solutions (95% D_2O, 5% MeOD-d_4). The ^{1}H NMR spectra were recorded at various time intervals at 310 K. The relative amounts of chlorido species or aqua adducts (determined by integration of peaks in ^{1}H NMR spectra) versus time were fitted

(18) Sheldrick, G. M. *SADABS Version 2006−1*, University of Göttingen: Göttingen, Germany, 2006.
(19) Altomare, A.; Cascarano, G.; Giacovazzo, C.; Guagliardi, A.; Polidori, G.; Camalli, M. *J. Appl. Crystallogr.* **1994**, *27*, 435.
(20) Betteridge, P. W.; Carruthers, J. R.; Cooper, R. I.; Prout, K.; Watkin, D. J. *J. Appl. Crystallogr.* **2003**, *36*, 1487.
(21) Sheldrick, G. M. *SHELXS-97*, University of Göttingen: Göttingen, Germany, 1997.
(22) Beurskens, P. T. B., G.; Bosman, W. P.; de Gelder, R.; Garcia-Granda, S.; Gould, R. O.; Israel, R.; Smits, J. M. M. *The DIRDIF96 Program System.* University of Nijmegen: Nijmegen, The Netherlands, 1996.
(23) Sheldrick, G. M. *SHELXL-97*, University Of Göttingen: Göttingen, Germany, 1997.

to appropriate equations for pseudo first-order kinetics using Origin version 7.5 (Microcal Software Ltd.) to give the half-lives and rate constants.

Rate of Arene Loss. The complexes were dissolved in MeOD-d_4 and diluted with D_2O to give ca. 100 μM solutions (95% D_2O, 5% MeOD-d_4). Arene loss with time was followed by ^{1}H NMR.

Computation. The initial coordinates of complexes used for the calculations were obtained directly from the X-ray crystal structures. Modifications to the structures were performed in Chemcraft (Version 1.5). The calculations were carried out using density functional theory (DFT) at the generalized gradient approximation (GGA) as implemented in the Amsterdam density functional (ADF)[24] program (version 2007.01). Geometries and energies were obtained by using the Becke Perdew gradient-corrected functional with scalar ZORA relativistic correction,[25−29] unless otherwise stated. The general numerical integration was 4.0. The frozen core approximation[30] was applied using triple-ζ polarization (TZP) bases, for all the atoms, apart from H atoms, with the orbitals up to and including the ones labeled in brackets: Ru[3d], Cl[2p], O[1s], N[1s] and C[1s]. Default convergence criteria were applied for self-consistent field (SCF) and geometry optimization. Geometries and energies were not confirmed with frequency calculations. The COSMO solvation model, as implemented in the ADF program, was used to simulate the aqueous environment with $\varepsilon = 78.4$ and a probe radius = 1.9 Å. The atomic radii used were Ru = 1.950, Cl = 1.725, O = 1.517, N = 1.608, C = 1.700 and H = 1.350. Single point calculations were carried out for the tha fragment of the cation of complex **10** [(η^6-tha)Ru(bipy(OH)O)(9-EtG-*N7*)]$^+$ and the fragment of the cation without tha. The energies of these two separate fragments were subtracted from the energy of the entire 1+ cation of complex **10**, in the single point calculation of the cation of **10** [(η^6-tha)Ru(bipy(OH)O)(9-EtG-*N7*)]$^+$, to obtain the total bonding energy of tha. The total bonding energy of tha is a sum of the bonding energy of the arene and Ru and the energy of the CH/π interaction between the arene and the chelating ligand (bipy(OH)O). The tha ligand in the crystal structure of **10** was rotated so as to allow $\pi-\pi$ interaction with the purine ring of the 9-EtG fragment and the geometry was optimized to give the minimum energy structure. After geometry optimization, a single point calculation was carried out again on the tha fragment of the modified cation of **10** and the fragment of the cation without tha. The energies of these two separate fragments were subtracted, in the single point calculation of the 1+ cation of modified **10**, from the energy of the entire cation of modified **10** [(η^6-tha)Ru(bipy(OH)O)(9-EtG-*N7*)]$^+$. The total bonding energy of tha obtained is in this case a sum of the bonding energy of the arene and Ru and the energy of the $\pi-\pi$ interaction. Upon geometry optimization, the atomic coordinates of the minimum energy structures were used in single point calculations.

Cancer Cell Growth Inhibition. Compounds were tested for growth inhibitory activity against the A2780 and A549 cancer cell lines at six different concentrations (100, 50, 10, 5, 1, and 0.1 μM), each in triplicate. Cisplatin was also tested as a control. The A2780 cancer cell line was maintained by growing the cells in RPMI medium supplemented with 5% fetal bovine serum, 1% penicillin/streptomycin, and 2 mM L-glutamine. The A549 cancer cell line was maintained by growing the cells in DMEM medium supplemented with 10% fetal bovine serum, 1% penicillin/streptomycin, and 2 mM L-glutamine.

A2780 cancer cells were plated out at a density of 5000 cells/well (±10%) on day 1. A549 cancer cells were plated out at a density 2000 cells/well (±10%) on day 2. On day 3, the test compound was dissolved in DMSO to give a stock solution of 20 mM, and serial dilutions were carried out in DMSO to give concentrations of complex in DMSO of 10, 2, 1, 0.2, and 0.02 mM. These were added to the wells to give the six test concentrations and a final concentration of DMSO of 0.5% (v/v). The wells were examined under the microscope to check for complete dissolution of the complex, and any precipitate present was noted. The cells were exposed to the complex for 24 h; then, after removal of the complex, fresh medium was added and the cells were incubated for 96 h of recovery time. The remaining biomass was then estimated by the sulforhodamine B assay.[31] IC_{50} values were calculated using XL-Fit version 4.0 (IDBS, Surrey, U.K.).

Metalation Reactions. CT DNA and plasmid DNAs were incubated with ruthenium or platinum complex in 10 mM $NaClO_4$ (pH = 6) at 310 K for 48 h in the dark, if not stated otherwise. The values of r_b (r_b values are defined as the number of atoms of the metal bound per nucleotide residue) were determined by FAAS.

Circular Dichroism (CD). Isothermal CD spectra of CT DNA modified by ruthenium complexes were recorded at 298 K in 10 mM $NaClO_4$ by using a Jasco J-720 spectropolarimeter equipped with a thermoelectrically controlled cell holder. The cell path length was 1 cm. Spectra were recorded in the range of 230−500 nm in 0.5 nm increments with an averaging time of 1 s.

DNA Melting. The melting curves of CT DNAs were recorded by measuring the absorbance at 260 nm. The melting curves of unmodified or ruthenated DNA were recorded in the medium containing 10 mM $NaClO_4$ with 1 mM Tris-HCl/0.1 mM EDTA, pH = 7.4 and 0.01 or 0.1 M $NaClO_4$. The melting temperature (t_m) was determined as the temperature corresponding to a maximum on the first-derivative profile of the melting curves. The t_m values could be thus determined with an accuracy of ±0.3 K.

Fluorescence Measurements. These measurements were performed on a Shimadzu RF 40 spectrofluorophotometer using a 1 cm quartz cell. Fluorescence measurements of CT DNA modified by Ru^{II} arene complexes, in the presence of EtBr, were performed at an excitation wavelength of 546 nm, and the emitted fluorescence was analyzed at 590 nm. The fluorescence intensity was measured at 298 K in 0.4 M NaCl to avoid secondary binding of EtBr to DNA.[32,33] The concentrations were 0.01 mg/mL for DNA and 0.04 mg/mL for EtBr, which corresponded to the saturation of all intercalation sites for EtBr in DNA.[32]

Replication Mapping of DNA Adducts. Replication with Sequenase 2 and electrophoretic analysis of the products of the DNA polymerization reaction were performed according to the protocols recommended by Amersham, Pharmacia and previously

(24) Te Velde, G.; Bickelhaupt, F. M.; Baerends, E. J.; Fonseca Guerra, C.; Van Gisbergen, S. J. A.; Snijders, J. G.; Ziegler, T. *J. Comput. Chem.* **2001**, *22*, 931–967.
(25) van Lenthe, E.; Baerends, E. J.; Snijders, J. G. *J. Chem. Phys.* **1993**, *99*, 4597–4610.
(26) van Lenthe, E.; Baerends, E. J.; Snijders, J. G. *J. Chem. Phys.* **1994**, *101*, 9783–9792.
(27) van Lenthe, E.; Ehlers, A.; Baerends, E. J. *J. Chem. Phys.* **1999**, *110*, 8943–8953.
(28) van Lenthe, E.; Snijders, J. G.; Baerends, E. J. *J. Chem. Phys.* **1996**, *105*, 6505–6516.
(29) van Lenthe, E.; Van Leeuwen, R.; Baerends, E. J.; Snijders, J. G *Int. J. Quantum Chem.* **1996**, *57*, 281–293.
(30) Baerends, E. J.; Ellis, D. E.; Ros, P. *Theor. Chim. Acta* **1972**, *27*, 339–354.
(31) Skehan, P.; Storeng, R.; Scudiero, D.; Monks, A.; McMahon, J.; Vistica, D.; Warren, J. T.; Bokesch, H.; Kenney, S.; Boyd, M. R. *J. Nat. Cancer Inst.* **1990**, *82*, 1107–1112.
(32) Butour, J. L.; Macquet, J. P. *Eur. J. Biochem.* **1977**, *78*, 455–463.
(33) Butour, J. L.; Alvinerie, P.; Souchard, J. P.; Colson, P.; Houssier, C.; Johnson, N. P. *Eur. J. Biochem.* **1991**, *202*, 975–980.

described.[34,35] The plasmid pSP73KB linearized by *Nde*I, which was used as a template for Sequenase 2, was modified with Ru^{II} complexes in 10 mM $NaClO_4$ at 310 K for 48 h in the dark. The level of ruthenation of DNA corresponded to $r_b = 0.001$ (r_b is defined as a number of ruthenium atoms coordinated per one nucleotide residue in DNA). Other details are in the text bellow.

Results

Synthesis and Characterization. The ligands used in this work are shown in Figure 1. The chlorido Ru^{II} arene complexes **1**−**8** (Figure 1) were synthesized as PF_6 salts or as neutral complexes in good yields by the reaction of [(η^6-arene)$RuCl_2$]$_2$ dimers and the appropriate chelating ligand in methanol. All the synthesized complexes were fully characterized by 1D ^{1}H NMR or 2D COSY and TOCSY ^{1}H NMR methods. The OH proton resonance from bipy(OH)O was shifted to very low field, at ∼18 ppm. The ^{1}H NMR resonances of the coordinated η^6-arenes are shifted upfield compared to the uncoordinated arenes.

The crystal structures of [(η^6-tha)Ru(bipy)Cl][PF_6] (**1**), [(η^6-tha)Ru(bipy(OH)O)Cl] (**2**) and [(η^6-ind)Ru(bipy-(OH)$_2$)Cl][PF_6] (**8**) are shown in Figure 2. The crystal structures of N-MeIm and 9-EtG adducts [(η^6-thn)Ru(bipy(OH)O)(N-MeIm)][PF_6] (**11**) and [(η^6-tha)Ru(bipy(OH)O)(9-EtG-*N7*)][PF_6] (**10**) are shown in Figure 3. The crystallographic data are listed in Table 1, and selected bond lengths and angles in Table 2. In all the complexes, Ru^{II} adopts the familiar 'three-legged piano-stool' geometry. It is π-bonded to the appropriate arene ligand and σ-bonded to the N atoms of the chelating ligand and Cl, or N-MeIm, or *N7* of 9-EtG. The Ru−Cl bond lengths in all the new chlorido Ru^{II} complexes are almost the same (∼2.4 Å). In the crystal structure of [(η^6-tha)Ru(bipy)Cl][PF_6]·H_2O (**1**·H_2O), the Ru−N (bipy) distances (2.085(2) and 2.0796(19) Å; Table 2) are significantly longer than Ru−N (bipy(OH)O) distances in [(η^6-tha)Ru(bipy(OH)O)Cl] (complex **2**; 2.0701(14) and 2.0659(13) Å; Table 2). In all the crystal structures, the Ru-arene centroid distances are similar (∼1.7 Å).

From the crystal structure of [(η^6-tha)Ru(bipy)-Cl][PF_6]·H_2O (**1**·H_2O), it can be seen (Figure 2A) that the outer ring of tha is tilted (tilt angle 41.41°) toward the chelating ligand. The space-filling and capped-stick models of **1**·H_2O (Figure 4, panels A and D, respectively) clearly show the presence of intramolecular CH/π interactions between CH protons of the outer ring of tha and the centers of the pyridine rings of the chelating ligand (distances 2.7 and 2.8 Å).

In the crystal structure of **2** (Figure 2B), one of the bipyridinediol oxygens is deprotonated, an intramolecular hydrogen bond forms (O82···H···O52; O−O distance 2.3886(19) Å), and the complex is neutral. The outer ring from the tricyclic-ring system of tha in the crystal structure of **2** is tilted by 36.90° toward the chelating ligand (Figure

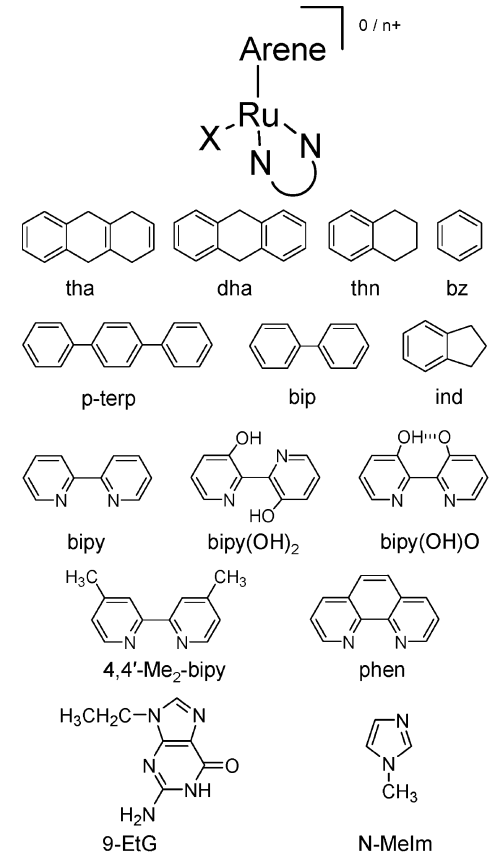

Complex	Arene	N-N	X
1	tha	bipy	Cl
2	tha	bipy(OH)O	Cl
3	dha	bipy(OH)O	Cl
4	thn	bipy(OH)O	Cl
5	bz	bipy(OH)O	Cl
6	p-terp	bipy(OH)O	Cl
7	bip	bipy(OH)O	Cl
8	ind	bipy(OH)$_2$	Cl
9	tha	bipy	9-EtG
10	tha	bipy(OH)O	9-EtG
11	thn	bipy(OH)O	N-MeIm
12	bz	bipy(OH)O	9-EtG
13	ind	4,4′-Me$_2$-bipy	Cl
14	ind	phen	Cl
15	bip	bipy	Cl
16	ind	bipy	Cl

Figure 1. General structures of the complexes studied in this work, as neutral or PF_6 salts. In complex **6**, Ru is bound to the terminal phenyl ring of *p*-terp.

(34) Burstyn, J. N.; HeigerBernays, W. J.; Cohen, S. M.; Lippard, S. J. *Nucleic Acids Res.* **2000**, *28*, 4237–4243.
(35) Intini, F. P.; Boccarelli, A.; Francia, V. C.; Pacifico, C.; Sivo, M. F.; Natile, G.; Giordano, D.; De Rinaldis, P.; Coluccia, M. *J. Biol. Inorg. Chem.* **2004**, *9*, 768–780.

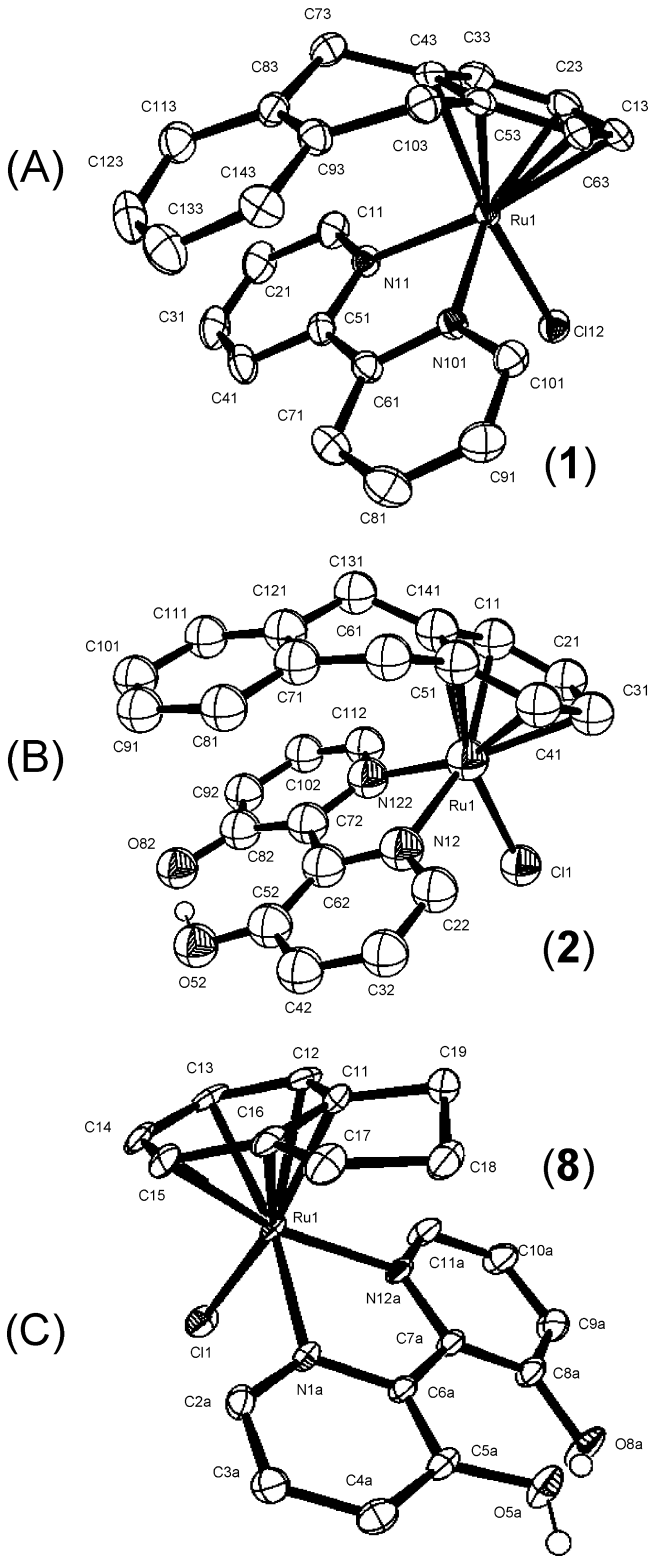

Figure 2. ORTEP diagrams for (A) cation of [(η^6-tha)Ru(bipy)Cl][PF_6]·H_2O (**1**·H_2O), (B) [(η^6-tha)Ru(bipy(OH)O)Cl] (**2**), and (C) cation of [(η^6-ind)Ru(bipy($OH)_2$)Cl][PF_6]·CH_3OH (**8**·CH_3OH), with 50% probability thermal ellipsoids. All hydrogens apart from OH hydrogen atoms from chelating ligands, bipy($OH)_2$ and bipy(OH)O, have been omitted for clarity.

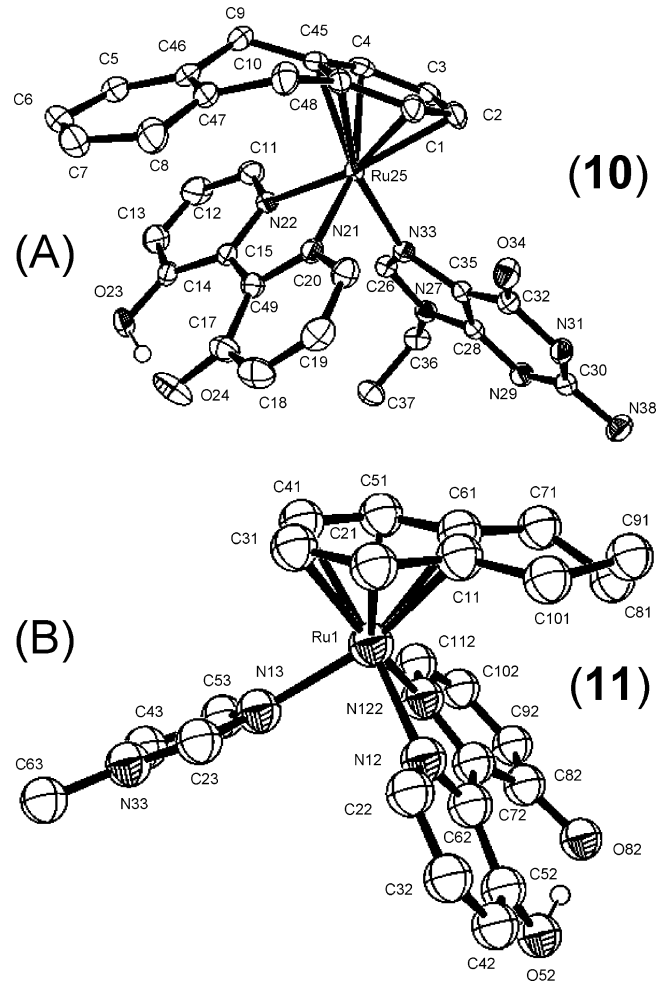

Figure 3. ORTEP diagrams for cations of (A) [(η^6-tha)Ru(bipy(OH)O)(9-EtG-*N7*)][PF_6]·CH_3OH (**10**·CH_3OH), and (B) [(η^6-thn)Ru(bipy(OH)O)(N-MeIm)][PF_6] (**11**) with 50% probability thermal ellipsoids. All hydrogens apart from OH hydrogen atom from chelating ligand bipy(OH)O have been omitted for clarity.

2B). The space-filling and capped-stick models (Figure 4B,E) clearly show the presence of intramolecular CH/π interactions between CH protons of the outer ring of tha and the centers of the pyridine rings of the chelating ligand bipy(OH)O (distances 2.8 and 2.9 Å).

The X-ray crystal structure of the cation of [(η^6-ind)Ru(bipy($OH)_2$)Cl][PF_6]·CH_3OH (**8**·CH_3OH, Figure 2C) shows a twisting of the pyridine rings of bipyridinediol (twist angle 17.31°) as well as intramolecular H-bonding involving the OH groups and intermolecular H-bonding involving methanol to give dimers in the unit cell (Figure 5A). The two oxygen atoms of the bipy($OH)_2$ ligand (O5A and O8A) are 2.532(4) Å apart.

[(η^6-Tha)Ru(bipy(OH)O)(9-EtG-*N7*)][PF_6] (**10**) crystallized with one molecule of solvent (CH_3OH) in the lattice per molecule of complex. One of the oxygens of the chelating ligand in the crystal structure of **10**·CH_3OH is deprotonated and an intramolecular hydrogen bond is formed between this oxygen (O24) and the hydrogen from the other oxygen (O23; Figure 3A). The two oxygen atoms are 2.389(3) Å apart. The outer ring from the coordinated tricyclic-ring system of tha is tilted (tilt angle 37.21°) toward the chelating bipy(OH)O ligand. The space-filling and capped-stick models (Figure 4C,F) show the presence of intramolecular CH/π interactions between CH protons of the outer ring of tha and

Table 1. X-ray Crystal Structure Data for Complexes **1**·H_2O, **2**, **8**·CH_3OH, **10**·CH_3OH and **11**

	1·H_2O	**2**	**8** cdtCH_3OH	**10**·CH_3OH	**11**
Formula	$C_{24}H_{24}ClF_6N_2OPRu$	$C_{24}H_{21}ClN_2O_2Ru$	$C_{20}H_{22}ClF_6N_2O_3PRu$	$C_{32}H_{34}F_6N_7O_4PRu$	$C_{24}H_{25}F_6N_4O_2PRu$
Molar mass	637.95	505.95	619.89	826.70	647.52
Crystal system	triclinic	monoclinic	triclinic	monoclinic	monoclinic
Crystal size/mm	0.42 × 0.25 × 0.14	0.40 × 0.18 × 0.11	0.37 × 0.25 × 0.12	0.23 × 0.12 × 0.09	0.44 × 0.40 × 0.18
Space group	$P\bar{1}$	$P2_1/n$	$P\bar{1}$	$P1\ 2_1/n1$	$P2_1/n$
Crystal	Yellow/block	Yellow/block	Orange/block	Brown/block	Yellow/block
a/Å	7.4422(3)	7.2697(2)	7.9858(10)	9.5526(2)	12.7776(2)
b/Å	11.8685(5)	16.7711(4)	12.1538(15)	10.8630(2)	13.4949(3)
c/Å	13.7805(6)	16.0993(4)	12.5825(16)	31.6240(7)	14.4729(3)
α/deg	94.960(2)	90	67.843(2)	90	90
β/deg	101.341(2)	99.6900(10)	83.718(2)	95.1740(10)	90.7780(10)
γ/deg	91.580(2)	90	83.549(2)	90	90
T/K	150	150(2)	150(2)	150	150(2)
Z	2	4	2	4	4
$R\ [F > 4\sigma\ (F)]^a$	0.0336	0.0250	0.0464	0.0408	0.0331
$R_w{}^b$	0.0868	0.0656	0.1248	0.0427	0.0845
GOF[c]	0.9159	1.077	1.051	1.0967	1.034
Δ*ρ* max and min,/eÅ^{-3}	0.81, −0.78	0.599, −0.380	2.784, −1.723	0.90, −0.57	0.879, −0.540

[a] $R = \sum||F_o| - |F_c||/\sum|F_o|$. [b] $R_w = [\sum w(F_o^2 - F_c^2)^2/\sum wF_o^2)]^{1/2}$. [c] GOF $= [\sum w(F_o^2 - F_c^2)^2/(n - p)]^{1/2}$, where n = number of reflections and p = number of parameters.

Table 2. Selected Bond Lengths (Å) and Angles (deg) for Complexes **1**, **2**, **8**, **10** and **11**

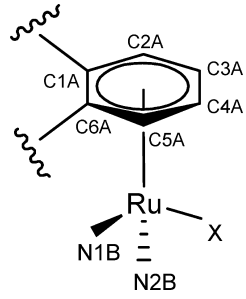

Bond/angle[a]	**1**	**2**	**8**	**10**	**11**
Ru−Cl	2.4047(6)	2.3958(4)	2.4118(8)	-	-
Ru−N13	-	-	-	-	2.0971(17)
Ru−N33	-	-	-	2.1233(19)	-
Ru−N1B	2.085(2)	2.0701(14)	2.080(3)	2.0786(19)	2.0706(16)
Ru−N2B	2.0796(19)	2.0659(13)	2.070(3)	2.077(2)	2.0736(16)
Ru−C1A	2.191(2)	2.1928(15)	2.200 (3)	2.195(2)	2.234(2)
Ru−C2A	2.215(2)	2.2083(15)	2.230(3)	2.225(2)	2.185(2)
Ru−C3A	2.215(2)	2.2073(16)	2.221(3)	2.220(2)	2.188(2)
Ru−C4A	2.199(2)	2.2189(17)	2.215(3)	2.217(2)	2.203(2)
Ru−C5A	2.192(2)	2.2124(16)	2.204(3)	2.206(2)	2.204(2)
Ru−C6A	2.193(2)	2.1934(15)	2.195(3)	2.201(2)	2.2270(19)
N2B−Ru−N1B	76.89(8)	76.49(5)	76.52(10)	76.27(7)	77.09(6)
N1B−Ru−Cl	85.85(6)	85.06(4)	87.15(7)	-	-
N1B−Ru−N13	-	-	-	-	88.08(6)
N1B−Ru−N33	-	-	-	85.71(7)	-
N2B−Ru−Cl	85.44(5)	87.03(4)	85.55(8)	-	-
N2B−Ru−N13	-	-	-	-	89.23(7)
N2B−Ru−N33	-	-	-	85.87(7)	-

[a] Atom labeling scheme used for purposes of comparison only. The crystallographic atom labeling schemes for individual complexes are different. X = Cl, N13 or N33.

the centers of the pyridine rings of bipy(OH)O (distances 2.8 and 3.0 Å).

In the crystal structure of [(η^6-thn)Ru(bipy(OH)O)(N-MeIm)][PF_6] (**11**), one of the oxygens of the bipydiol ligand (O82) is again deprotonated (Figure 3B) and an intramolecular hydrogen bond is formed between this oxygen and the hydrogen from the other oxygen (O52). The two oxygen atoms are 2.390(3) Å apart. Ru is *σ*-bonded to N13 of *N*-methylimidazole. Neither intra- nor intermolecular $\pi-\pi$ stacking nor CH/π interactions are observed in the crystal structure of **11**. The noncoordinated ring of thn is disordered and bipy(OH)O ligand is twisted (by 14.43°), as a result of the hydrogen bond formed between O82 of bipy(OH)O of one molecule and the C43H hydrogen of *N*-methylimidazole of another molecule (Figure 5B).

pH Dependence. To determine the pK_a values of the OH protons of the bipyridinediol chelating ligand without the complication of deprotonation of coordinated water (aquation of chlorido complex), the N-MeIm adduct of [(η^6-thn)Ru-(bipy(OH)O)Cl] (**4**) was prepared (complex **11**). ^{1}H NMR spectra of [(η^6-thn)Ru(bipy(OH)O)(N-MeIm)][PF_6] (**11**) in DMSO-d_6 showed a peak at 17.88 ppm corresponding to the O−H···O proton from bipy(OH)O. ^{1}H NMR spectra of complex **11** in D_2O were recorded over the pH* range 2−10.

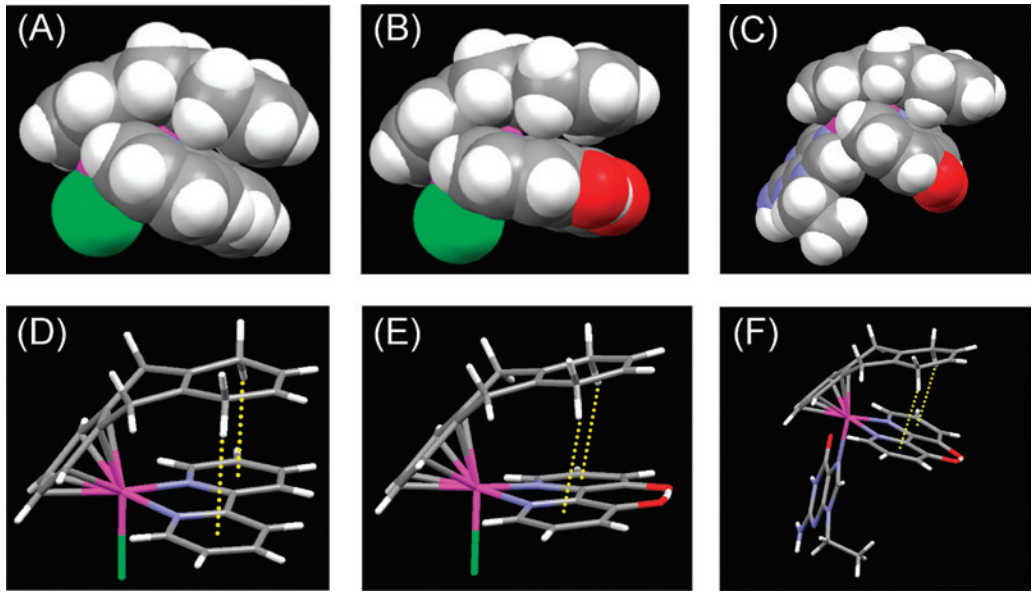

Figure 4. CH/π interactions in tha complexes **1**, **2** and **10**. Space-filling and capped-stick models (A and D) the cation of [(η^6-tha)Ru(bipy)Cl][PF_6]·H_2O (**1**·H_2O), (B and E) [(η^6-tha)Ru(bipy(OH)O)Cl] (**2**) and (C and F) cation of [(η^6-tha)Ru(bipy(OH)O)(9-EtG-*N7*)][PF_6]·CH_3OH (**10**·CH_3OH), showing interaction between CH protons from the outer ring of tha and the centers of the π-systems of the chelating ligands.

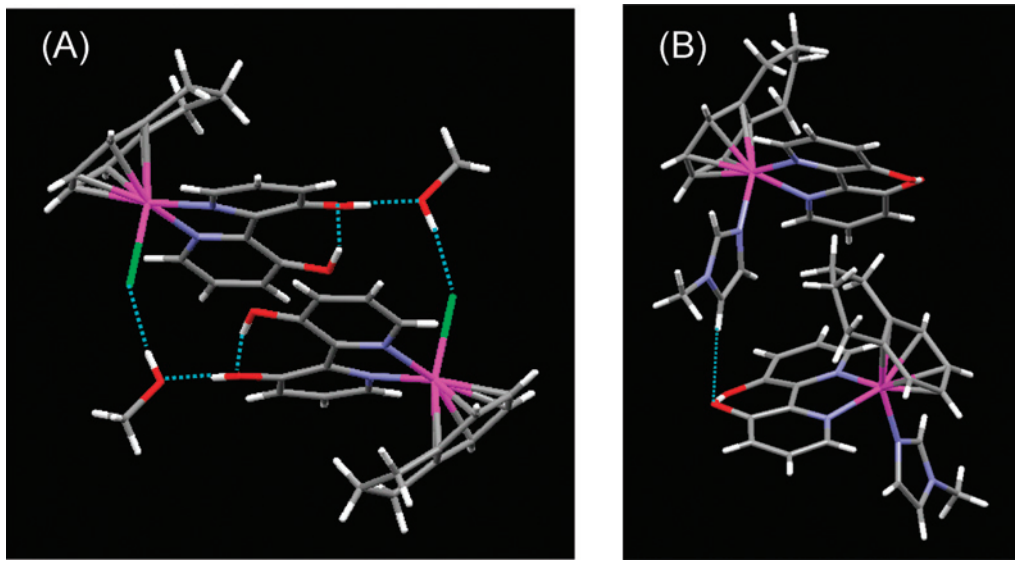

Figure 5. (A) H-bonding involving the OH groups of [(η^6-ind)Ru(bipy($OH)_2$)Cl][PF_6]·CH_3OH (**8**·CH_3OH) giving rise to dimers in the unit cell. (B) Twisting of the bipy(OH)O ligand in [(η^6-thn)Ru(bipy(OH)O)(N-MeIm)][PF_6] (**11**) as a result of H-bond formation between O82 from bipy(OH)O of one molecule and C43H from N-MeIm of another molecule.

None of the peaks shifted as a function of pH within this range, indicating that the form of the chelated ligand does not change. Therefore, it is reasonable to assume that, at physiological pH (pH = 7), the ligand is present in the deprotonated form, bipy(OH)O.

Aqueous Solution Chemistry. The hydrolysis of complexes **4**, **7**, **8**, and **13**−**16** was studied at 310 K using UV−vis or by ^{1}H NMR spectroscopy (complex **4**). Because of the small amount of sample required, in general, it was more convenient to follow hydrolysis by UV−vis spectroscopy.

The time dependence of the absorbance of the complexes followed pseudo first-order kinetics (Figure 6A) in each case. ESI-MS spectra were consistent with the formation of the aqua complex as the product (observed peaks: [(η^6-thn)Ru(bipy(OH)O)H_2O]$^{1+}$ -H_2O calc. *m*/*z* 421.1, found *m*/*z* 421.3; [(η^6-bip)Ru(bipy(OH)O)H_2O]$^{1+}$ -H_2O calc. *m*/*z* 443.0, found *m*/*z* 443.1; [(η^6-ind)Ru(bipy(OH)O)H_2O]$^{1+}$ -H_2O calc. *m*/*z* 407.0, found *m*/*z* 407.2; [(η^6-ind)Ru(4,4′-Me_2-bipy)H_2O]$^{2+}$ -H_2O -H^+ calc. *m*/*z* 403.1, found *m*/*z* 403.2; [(η^6-ind)Ru(phen)H_2O]$^{2+}$ -H_2O -H^+ calc. *m*/*z* 399.0, found *m*/*z* 399.1; [(η^6-bip)Ru(bipy)H_2O]$^{2+}$ -H_2O -H^+ calc. *m*/*z* 411.0, found *m*/*z* 411.1; [(η^6-ind)Ru(bipy)H_2O]$^{2+}$ -H_2O -H^+ calc. *m*/*z* 375.0, found *m*/*z* 375.1 for the aqua adducts of complexes **4**, **7**, deprotonated **8**, **13**, **14**, **15** and **16**, respectively).

^{1}H NMR spectra of **4** in 5% MeOD-d_4/95% D_2O (for which hydrolysis was also monitored using UV−vis spectroscopy) initially contained one major set of peaks (chlorido species), and then, a second set of peaks increased in intensity with time. The new set of peaks has the same chemical shifts as those of the aqua adduct under the same conditions (310

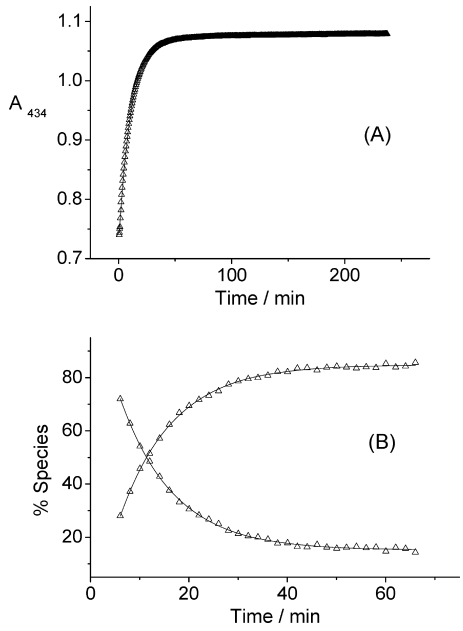

Figure 6. (A) Dependence of the absorbance at 434 nm over ca. 4 h during aquation of complex **4** at 310 K. (B) Time dependence of the percentage of chlorido and aqua species during aquation of complex **4** at 310 K followed by ^{1}H NMR.

Table 3. Hydrolysis Data for Complexes **4**, **7**, **8**, **13**, **14**, **15** and **16** at 310 K

complex		$10^3 \cdot k_{obs}$ (min^{-1})[a]	$t_{1/2}$ (min)
[(η^6-thn)Ru(bipy(OH)O)Cl]	(**4**)	91.8 ± 0.4[b]	7.55
		91.6 ± 1.4[c]	7.57
[(η^6-bip)Ru(bipy(OH)O)Cl]	(**7**)	46.3 ± 0.2[b]	14.95
[(η^6-ind)Ru(bipy(OH)O)Cl][d]	(**8**)	164.6 ± 1.0[b]	4.21
[(η^6-ind)Ru(4,4′-Me_2-bipy)Cl][PF_6]	(**13**)	113.0 ± 2.0[b]	6.30
[(η^6-ind)Ru(phen)Cl][PF_6]	(**14**)	75.1 ± 1.2[b]	9.24
[(η^6-bip)Ru(bipy)Cl][PF_6]	(**15**)	93.3 ± 0.8[b]	7.43
[(η^6-ind)Ru(bipy)Cl][PF_6]	(**16**)	121.0 ± 1.0[b]	5.73

[a] The errors quoted are fitting errors. [b] Determined by UV−vis spectroscopy for a 50 μM solution in 95% H_2O, 5% MeOH. [c] Determined by ^{1}H NMR spectroscopy in 95% D_2O, 5% MeOD-d_4 [d] Species present in aqueous solution; synthesized as [(η^6-ind)Ru(bipy($OH)_2$)Cl][PF_6].

K, 100 μM solutions in 5% MeOD-d_4/95% D_2O). The aqua adduct was prepared by treatment of **4** with $AgNO_3$ in water at room temperature overnight and removal of AgCl by filtration. The time dependence of the increase in concentration of aqua adduct or decrease in concentration of chlorido species followed first-order kinetics (Figure 6B), and the corresponding rate constant is listed in Table 3 together with rate constants determined using UV-vis spectroscopy.

For complexes [(η^6-bip)Ru(bipy(OH)O)Cl] (**7**) and [(η^6-bip)Ru(bipy)Cl][PF_6] (**15**), separate sets of peaks were observed in ^{1}H NMR spectra (in 5% MeOD-d_4/95% D_2O) for products which had undergone arene-loss during the aquation. After 24 h, 33% of **7** and 46% of **15** had undergone arene loss.

The hydrolysis rates for the complexes which did not undergo arene loss were determined over a period of 4 h. The rate constants for bip complexes that underwent arene loss were determined over the period of time before the onset of arene loss (80 min, detected by NMR). It can be seen that hydrolysis of the neutral bip complex **7** containing bipy(OH)O as chelating ligand ($t_{1/2}$ = 14.95 min) is twice as

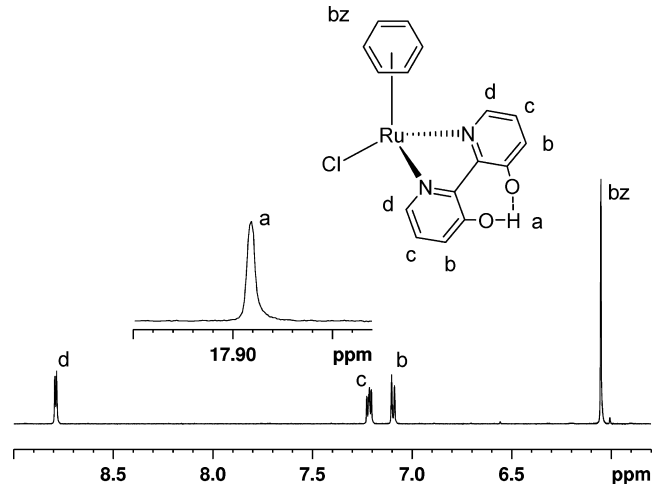

Figure 7. Low field region of the ^{1}H NMR spectrum of [(η^6-bz)Ru(bipy(OH)O)Cl] (**5**) in DMSO-d_6. Inset: shows resonance of H-bonded proton from bipy(OH)O ligand.

slow as for the positively charged bip complex **15** containing bipy as chelating ligand ($t_{1/2}$ = 7.43 min), Table 3.

Aqueous solutions of [(η^6-ind)Ru(bipy($OH)_2$)Cl][PF_6] (**8**) were found to be acidic immediately after dissolution (1 mM, pH ∼ 3) consistent with the release of a proton from bipy($OH)_2$. Aqueous solutions of [(η^6-thn)Ru(bipy(OH)O)Cl] (**4**) were approximately neutral in pH, consistent with a lack of proton dissociation.

Interactions with 9-EtG. Attempts were made to prepare 9-EtG adducts of the bipy complex **1** and the bipy(OH)O complexes **2** and **5**. Reactions were carried out in water for 2 h at 310 K. The ^{1}H NMR spectrum of the product from the reaction of complex **1** with 9-EtG, in DMSO-d_6 showed that 90% of complex **1** had reacted with 9-EtG to form [(η^6-tha)Ru(bipy)(9-EtG-*N7*)][PF_6]$_2$ (complex **9**). Peaks assigned to bound 9-EtG in complex **9** are shifted to high field in comparison to those of free 9-EtG, the H8 peak (7.4 ppm) by 0.35 ppm. The ^{1}H NMR spectrum of the product in MeOH-d_4 showed that 98% of complex **2** had reacted with 9-EtG to form [(η^6-tha)Ru(bipy(OH)O)(9-EtG-*N7*)][PF_6] (complex **10**). Peaks assigned to bound 9-EtG in complex **10** were again shifted to high field compared to those of free 9-EtG, the H8 peak (7.12 ppm) by 0.63 ppm. The ^{1}H NMR spectrum of complex **5** in DMSO-d_6 is shown in Figure 7 and the ^{1}H NMR spectrum of the product from reaction of **5** with 9-EtG ([(η^6-bz)Ru(bipy(OH)O)(9-EtG-*N7*)][PF_6], complex **12**) in DMSO-d_6 in Figure 8. Under the conditions of this reaction, almost complete binding of 9-EtG to complex **5** occurred. Peaks assignable to bound 9-EtG in complex **12** are again shifted to high field compared to the peaks of free 9-EtG, the H8 peak (7.01 ppm) by 0.74 ppm.

Computation. The minimum energy structures of chlorido complexes [(η^6-ind)Ru(bipy($OH)_2$)Cl][PF_6] (**8**), [(η^6-ind)Ru(bipy($Me)_2$)Cl][PF_6] (**13**) and [(η^6-ind)Ru(bipy)-Cl][PF_6] (**16**) obtained from DFT calculations are shown in Figure 9. The total bonding energy of tha in the optimized structure of [(η^6-tha)Ru(bipy(OH)O)(9-EtG-*N7*)]$^+$ (cation of **10**, where the arene is interacting with the chelating ligand through the intramolecular CH/π interaction) is −313.4 kJ/mol, which is 7.5 kJ/mol lower than the bonding energy of

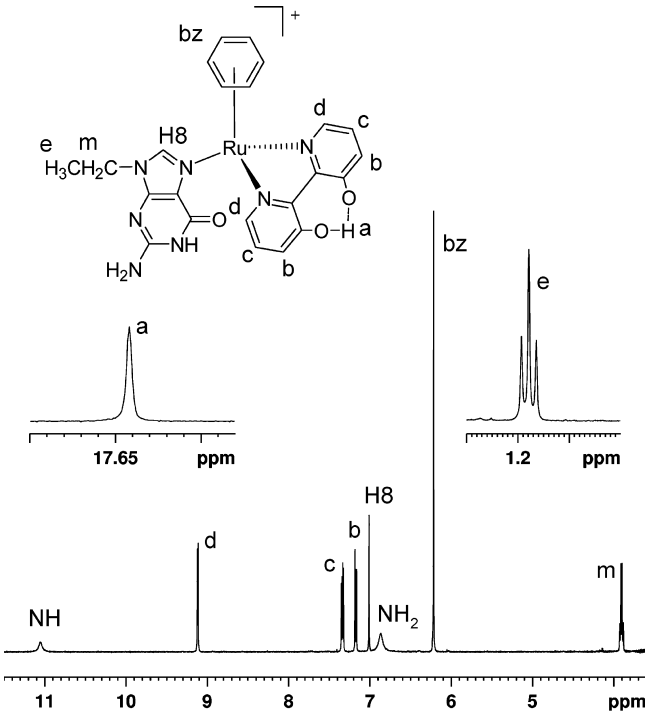

Figure 8. Low field region of the ^{1}H NMR spectrum of [(η^6-bz)Ru(bipy(OH)O)(9-EtG-*N7*)][PF_6] (**12**) in DMSO-d_6. Low field inset: resonance for H-bonded proton from chelating ligand. High field inset: CH_3 resonance of 9-Et-G.

tha in the optimized structure of modified complex **10** (−305.9 kJ/mol), in which there is an arene/9-EtG intramolecular $\pi-\pi$ interaction. The minimum energy structures of complex **10** and modified complex **10** are shown in Figure 10. To determine the effect of bipy substituents on the electron density on ruthenium, the Veronoi Deformation Density (VDD) method for computing atomic charges was used. This method has been used previously for transition metals such as Cr and Fe, in complexes $Cr(CO)_6$ and $Fe(CO)_5$.[36] Charges on Ru in the bipy$(OH)_2$ complex **8**, bipy$(Me)_2$ complex **13** and bipy complex **16** were found to be similar, with values of +0.268 au for **8** and **13** and +0.270 au for complex **16**. For deprotonated complex **8**, [(η^6-ind)Ru(bipy(OH)O)Cl] the charge on Ru was +0.271 au.

Cancer Cell Growth Inhibition. The IC_{50} values for chlorido complexes (**1**−**8**) against the A2780 human ovarian and A549 human lung cancer cell lines are given in Table 4. In general, the complexes were more active against the A2780 human ovarian cancer cells than against A549 human lung cancer cells (IC_{50} values 7−65 μM for A2780 ovarian cells, and 21−62 μM for A549 lung cells). The most potent complex against A2780 cells [(η^6-thn)Ru(bipy(OH)O)Cl] (**4**) had an IC_{50} value of 7 μM, comparable to that of cisplatin (5 μM) under the same conditions. In general, the most active complexes against the A2780 ovarian cancer cell line contain the most extended arenes in the order thn, tha > dha, ind > *p*-terp > bip > bz. An exception is the tha/bipy complex **1**, which is inactive against both A2780 and A549 cells (IC_{50} values >100 μM, Table 4). Complexes **5** and **7** containing

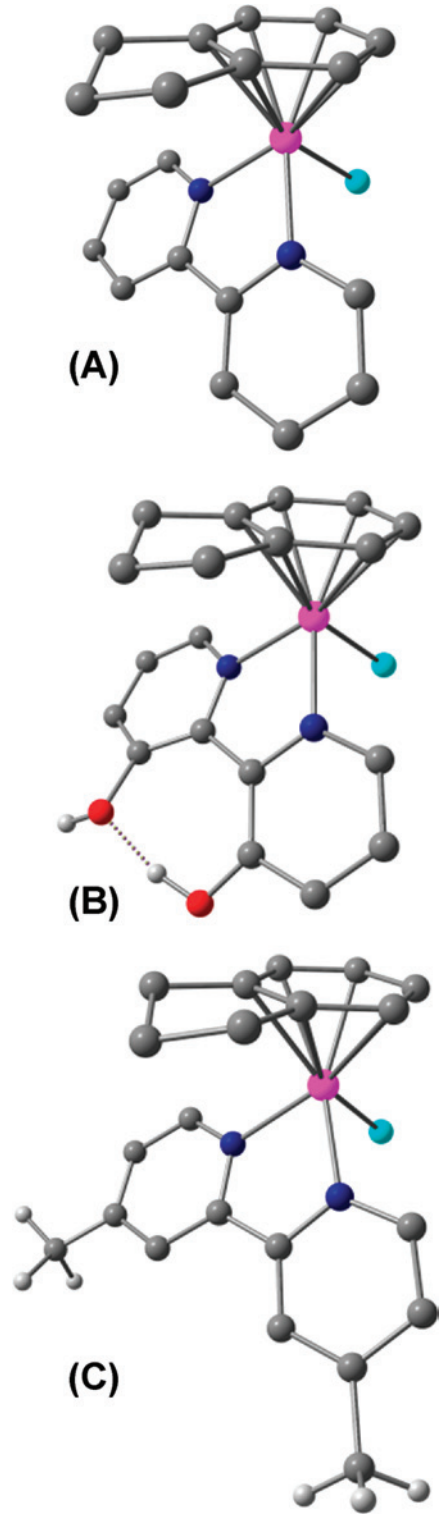

Figure 9. Optimized geometries of cations of complexes (A) [(η^6-ind)Ru(bipy)Cl][PF_6] (**16**), (B) [(η^6-ind)Ru(bipy$(OH)_2$)Cl][PF_6] (**8**) and (C) [(η^6-ind)Ru(bipy$(Me)_2$)Cl][PF_6] (**13**). All the H-atoms were omitted for clarity apart from the H-atoms of the substituents on bipy.

bz and bip as arenes, respectively, and bipy(OH)O as chelating ligand were also inactive against A549 cells. The most active complex against this cell line was [(η^6-tha)Ru(bipy(OH)O)Cl] (**2**) with an IC_{50} value of 21 μM. The IC_{50} values for bipy(OH)O complexes showed the following dependence on the arene: thn, tha < dha, ind < *p*-terp (Table 4).

(36) Guerra, C. F.; Handgraaf, J.-W.; Baerends, E. J.; Bickelhaupt, F. M. *J. Comput. Chem.* **2003**, *25*, 189–210.

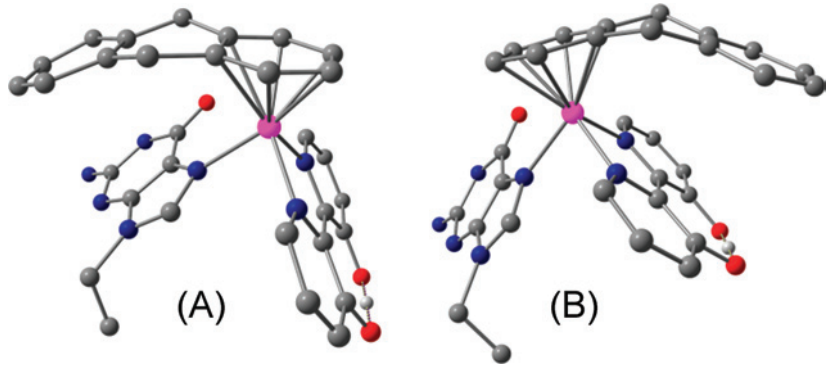

Figure 10. Optimized geometries of cations of complexes (A) modified **10** where tha is interacting with 9-EtG through the $\pi-\pi$ interaction, and (B) [(η^6-tha)Ru(bipy(OH)O)(9-EtG-*N7*)][PF_6] (**10**), where tha is interacting with bipy(OH)O through CH/π interaction.

Table 4. IC_{50} Values for Ruthenium(II) Arene Complexes against the A2780 Human Ovarian and A549 Human Lung Cancer Cell Lines

complex		IC_{50} (μM) A2780	IC_{50} (μM) A549	% arene loss (24 h, 310 K)[a]
[(η^6-tha)Ru(bipy)Cl][PF_6]	(**1**)	>100 ± 9	>100 ± 13	0
[(η^6-tha)Ru(bipy(OH)O)Cl]	(**2**)	8 ± 2	21 ± 4	0
[(η^6-dha)Ru(bipy(OH)O)Cl]	(**3**)	17 ± 3	38 ± 4	0
[(η^6-thn)Ru(bipy(OH)O)Cl]	(**4**)	7 ± 1	24 ± 4	0
[(η^6-bz)Ru(bipy(OH)O)Cl]	(**5**)	65 ± 7	>100 ± 10	0
[(η^6-p-terp)Ru(bipy(OH)O)Cl]	(**6**)	21 ± 3	62 ± 4	–[b]
[(η^6-bip)Ru(bipy(OH)O)Cl]	(**7**)	40 ± 8	>100 ± 9	33
[(η^6-ind)Ru(bipy(OH)O)Cl][c]	(**8**)	18 ± 3	39 ± 5	0
[(η^6-bip)Ru(bipy)Cl][PF_6]	(**15**)	>100 ± 10[d]	-	46
cisplatin		5 ± 1	5 ± 1	-

[a] Determined by ^{1}H NMR spectroscopy in 95% D_2O, 5% MeOH-d_4. [b] Solubility too low to determine arene loss by NMR. [c] Species present under test conditions; synthesized as [(η^6-ind)Ru(bipy($OH)_2$)Cl][PF_6]. [d] Previously reported.[10]

Binding to Calf Thymus (CT) DNA. The extent of binding of complexes [(η^6-ind)Ru(bipy)Cl][PF_6] (**16**) and [(η^6-ind)Ru(bipy($OH)_2$)Cl][PF_6] (**8**, under the experimental conditions as neutral [(η^6-ind)Ru(bipy(OH)O)Cl]) to CT DNA was determined at an r_i (molar ratio of free complex to nucleotide phosphate) ratios of 0.02−0.16 in 10 mM $NaClO_4$ at 310 K after 48 h of the reaction in the dark. Complexes **16** and **8** were incubated with the CT DNA for 48 h and rapidly cooled, DNA containing bound complex was precipitated out by addition of ethanol, and the content of free Ru in the supernatant was determined by FAAS. Intriguingly, both complexes bind to a relatively small extent (only ∼40% and ∼10% of **16** and **8**, respectively, after 48 h).

The binding experiments carried out in this work indicated that modification reactions resulted in the irreversible coordination of Ru^{II} arene complexes to CT DNA, which thus facilitated sample analysis. Hence, it was possible to prepare samples of DNA modified by complexes **16** or **8** at a preselected value of r_b. Thus, except where stated, samples of DNA modified by Ru^{II} arene complexes and analyzed further by biophysical or biochemical methods were prepared in 10 mM $NaClO_4$ at 310 K. After 48 h of the reaction of DNA with complexes, the samples were precipitated in ethanol and dissolved in the medium necessary for a particular analysis, and the r_b value in an aliquot of this sample was checked by FAAS. In this way, all analyses described in the present paper were performed in the absence of unbound (free) complex.

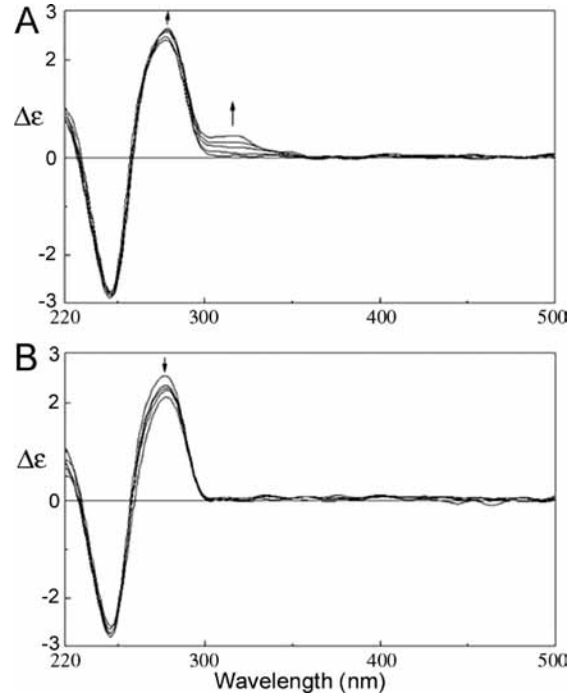

Figure 11. Circular dichroism (CD) spectra of calf thymus DNA (1×10^{-4} M, the concentration is related to the phophorus content) modified by complexes **16** or **8**; the medium was 10 mM $NaClO_4$, pH = 6. (A) DNA was modified by complex **16** at r_b = 0, 0.006, 0.026, 0.040, 0.056. (B) DNA was modified by complex **8** at r_b = 0, 0.017, 0.031, 0.044, 0.084 (curves 1−5, respectively). The arrows in panels A and B show a change of CD with increasing r_b value.

Circular Dichroism (CD). To gain further information, we also recorded CD spectra of CT DNA modified by **16** and **8** (Figure 11). CD spectral characteristics were compared for CT DNA in the absence and in the presence of **16** and **8** at r_b values in the range of 0.006−0.056 and 0.017−0.084, respectively. Upon binding of these compounds to CT DNA, the conservative CD spectrum normally found for DNA in canonical B-conformation transforms at wavelengths below 300 nm. There was a slight, but significant increase or decrease in the intensity of the positive band around 280 nm if DNA was modified by **16** or **8**, respectively. This increase or decrease was similar to that observed if DNA was under identical conditions modified by cisplatin or ineffective transplatin, respectively.[37] On the basis of the analogy with the changes in the CD spectra of DNA modified by cisplatin and clinically ineffective transplatin,[37] it might

be suggested that the binding of **16** results in conformational alterations to double-helical DNA of nondenaturational character, similar to those induced in DNA by conventional antitumor cisplatin. On the other hand, the binding of **8** results in conformational alterations to DNA of denaturational character, similar to those induced in DNA by clinically ineffective transplatin.

Complexes **16** and **8** have no intrinsic CD signals as they are achiral so that any CD signal above 300 nm can be attributed to the interaction of complexes with DNA. Below 300 nm, any change from the DNA spectrum is due either to the DNA induced CD (ICD) of the metal complex or the metal complex induced perturbation of the DNA spectrum. The signature of complex **16** bound to CT DNA is a strong positive ICD centered at 320 nm (Figure 11A). On the other hand, the signature of complex **8** bound to CT DNA includes no such ICD (Figure 11B).

CT DNA was also modified by **16** at $r_i = 0.13$ (the sample was incubated for 24 h under conditions specified in Experimental Section). The sample was divided into two parts, one was left (no additional treatment) and the second part was exhaustively dialyzed so that only strongly bound molecules of **16** remained in this sample. The r_b value estimated for this (dialyzed) sample was 0.06. This implies that DNA modified at $r_i = 0.13$ contained the same amount of Ru adducts firmly (presumably coordinatively) bound to DNA as the dialyzed sample modified at $r_b = 0.06$ and the other molecules of **16** were either not bound or were bound noncovalently. In order to distinguish between the latter two possibilities, CD spectra of both samples (dialyzed and nondialyzed) were recorded (Figure S1 in Supporting Information). In the case of the nondialyzed sample, the presence of molecules of **16** not strongly bound results in the enhancement of the induced CD centered at around 320 nm. This implies that at least some of the molecules become oriented as a consequence of their noncovalent interactions with DNA. In other words, this experiment demonstrates that the molecules of **16**, which are not strongly (coordinatively) bound, can interact with DNA via noncovalent binding. When the same experiment was performed with complex **8**, no differences in CD spectra of dialyzed and nondialyzed samples were observed.

DNA Melting. CT DNA was modified by [(η^6-ind)Ru(bipy)Cl][PF_6] (**16**) and [(η^6-ind)Ru(bipy($OH)_2$)Cl][PF_6] (**8**, under the experimental conditions as neutral [(η^6-ind)Ru(bipy(OH)O)Cl]) to the value of $r_b = 0.06$ and 0.08, respectively, in 10 mM $NaClO_4$ at 310 K for 48 h. The samples were divided into two parts and in one part the salt concentration was further adjusted by addition of $NaClO_4$ to 0.1 M. Hence, the melting curves for DNA modified by **16** and **8** were measured in the two different media, at low and high salt concentrations. The effect on the melting temperature (t_m) is dependent on the salt concentration. At both high and low salt concentration (0.01 and 0.1 M), modification of DNA by **16** and **8** affected t_m only very slightly (t_m was changed by less than 1 K). Thus, the melting behavior of DNA was affected by **16** and **8** only negligibly.

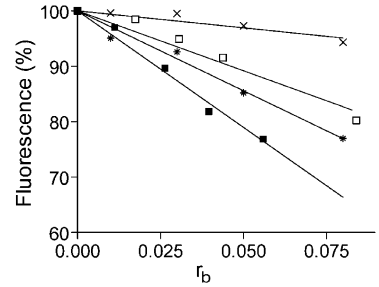

Figure 12. Plots of the EtBr fluorescence versus r_b for DNA modified by cisplatin, [PtCl(dien)]Cl and Ru^{II} arene complexes in 10 mM $NaClO_4$ at 310 K for 48 h: (x), [PtCl(dien)]Cl; (*), cisplatin; (■), complex **16**; (□), complex **8**. Data points measured in triplicate varied on average ± 3% from their mean.

Ethidium Bromide (EtBr) Fluorescence. The ability of complexes to displace the DNA intercalator EtBr from CT DNA was probed by monitoring the relative fluorescence of the EtBr−DNA adduct after treating the DNA with varying concentrations of **16** or **8**. Figure 12 shows a plot of relative fluorescence versus r_b for complexes **16** and **8**, cisplatin and monofunctional [PtCl(dien)]Cl. The adducts of both monofunctional Ru^{II} arene complexes competitively replaced intercalated EtBr markedly more effectively than the adducts of monofunctional [PtCl(dien)]Cl and the adducts of **16** even more than the adducts of bifunctional cisplatin. Thus, the ability of complex **16** to displace the DNA intercalator EtBr from CT DNA was considerably greater than that of complex **8**.

Replication Mapping of the Ru^{II} Adducts in the DNA Fragment. Further investigations were aimed at finding the sites in natural DNA in which the adducts were formed during the reaction with [(η^6-ind)Ru(bipy)Cl][PF_6] (**16**) or [(η^6-ind)Ru(bipy($OH)_2$)Cl][PF_6] (**8**, under the experimental conditions as neutral [(η^6-ind)Ru(bipy(OH)O)Cl]). Previous work has shown that the *in vitro* DNA synthesis by DNA polymerases on DNA template modified by various platinum and ruthenium complexes is terminated at the level of the adducts.[38−41] A similar approach was employed in the present work.

The primer extension footprinting assay was used to determine the sites of adducts of **16** or **8**. The pSP73KB plasmid (with a random natural nucleotide sequence) linearized by *Nde*I (isolated from the agarose gel) was incubated with **16** or **8** for 48 h at 310 K; the level of the modification was relatively low and corresponded to $r_b = 0.001$. After alkaline denaturation, the DNA samples were primed with SP6 primer supplied by the manufacturer and new DNA was synthesized by Sequenase 2 DNA polymerase in the presence of [α-^{32}P]dATP and unlabeled dNTPs. The products of DNA

(37) Brabec, V.; Kleinwächter, V.; Butour, J. L.; Johnson, N. P. *Biophys. Chem.* **1990**, *35*, 129–141.

(38) Comess, K. M.; Burstyn, J. N.; Essigmann, J. M.; Lippard, S. J. *Biochemistry* **1992**, *31*, 3975–3990.

(39) Novakova, O.; Kasparkova, J.; Malina, J.; Natile, G.; Brabec, V. *Nucleic Acids Res.* **2003**, *31*, 6450–6460.

(40) Moriarity, B.; Novakova, O.; Farrell, N.; Brabec, V.; Kasparkova, J. *Arch. Biochem. Biophys.* **2007**, *459*, 264–272.

(41) Novakova, O.; Kasparkova, J.; Vrana, O.; van Vliet, P. M.; Reedijk, J.; Brabec, V. *Biochemistry* **1995**, *34*, 12369–12378.

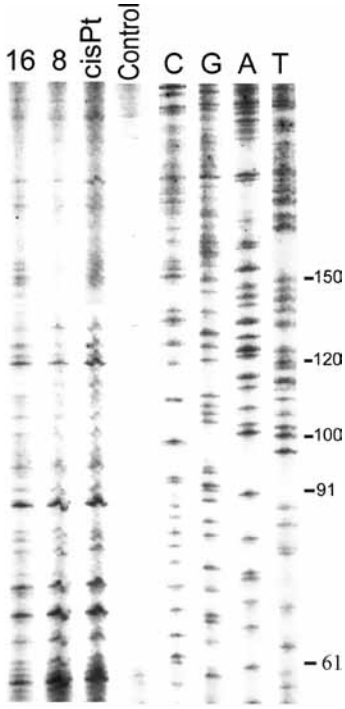

Figure 13. Autoradiogram of 6% polyacrylamide/8 M urea sequencing gel showing inhibition of DNA synthesis by Sequeanase 2 on linearized pSP73KB plasmid. The DNA was incubated with **16** or **8** at 310 K in 10 mM $NaClO_4$ for 48 h, $r_b = 0.001$. Lanes: Control, relative to the unmetallated template; **16**, **8**, and cisPt, relative to the DNA globally modified by **16**, **8**, and cisplatin, respectively; A, T, G, and C are relative to chain terminated marker DNAs.

polymerization were separated by electrophoresis on a 6% polyacrylamide/8 M urea denaturing gel in parallel to a sequence ladder obtained using an untreated control DNA and the sequence specificity of the Ru^{II} adduct formation was determined to the exact base pair. *In vitro* DNA synthesis on DNA templates containing the adducts of **16** or **8** generated a population of DNA fragments, indicating that the adducts of both ruthenium complexes effectively terminate DNA synthesis (Figure 13, lanes **16** and **8**). Strong and medium intensity bands (Figure 13, lanes **16** and **8**) were taken to indicate the sites of preferential formation of DNA adducts of **16** or **8**. The sequence analysis of the termination sites produced by both ruthenium complexes suggests a strong sequence preference for sites similar to those found for cisplatin (Figure 13, lane cisPt), that is, mainly for dG sites.

Discussion

We have observed previously a loss of cytotoxicity toward cancer cells for complexes of the type $[(\eta^6\text{-arene})Ru(en)Cl]^+$ when en, a σ-donor, is replaced by 2,2′-bipyridine.[10] Bipyridines contain two σ-donor nitrogens, and a fully conjugated π-system which makes them strong π-acceptors. Incorporation of methyl, hydroxymethyl or methylester groups in the 4,4′ positions of bipyridine did not restore activity. Loss of activity could arise from the absence of NH groups, which are known to stabilize nucleobase adducts through strong H-bonding between an NH of en and C6O from the guanine

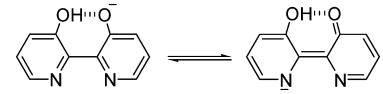

Figure 14. Tautomeric forms of bipy(OH)O.

(G) nucleobase,[42] or from the back-donation of electron density from Ru^{II} onto bipyridine as a π-acceptor, that would make the metal center more acidic compared to en analogues. This could have an effect on the binding of these complexes to DNA.

Complexes containing 2,2′-bipyridine-3,3′-diol (bipy-$(OH)_2$) as the chelating ligand showed a dramatic increase in anticancer activity compared to the other bipyridine analogues (Table 4).

Synthesis and Characterization. N, N-chelation of bipy$(OH)_2$ without deprotonation creates steric-crowding and distortion of ligand planarity, as observed in the crystal structure of $[(\eta^6\text{-ind})Ru(bipy(OH)_2)Cl]^+$ (**8**), where the pyridine rings are twisted by 17.31°, and previously for complexes of 3,3′-dimethyl-2,2′-bipyridine.[43] Chelation of bipyridine derivatives to a metal lowers the energy of the form in which the rings of the bipyridine are coplanar,[44−46] and the deprotonation of bipy$(OH)_2$ as a chelating ligand is favored as it leads to planarity of the ligand. Furthermore, for 2,2′-bipyridines with substituents in the 3,3′-positions, cyclization can occur when substituents are able to react, as observed for $-CO_2CH_2CF_3$ and $-CONHCH_2C_6H_5$ substituents that form $-CO(NCH_2C_6H_5)OC-$ with release of CF_3CH_2OH.[47]

CH/π interactions between the arene and the bipyridine ligand were observed in the crystal structures of $[(\eta^6\text{-tha})Ru(bipy)Cl][PF_6]$ (**1**), $[(\eta^6\text{-tha})Ru(bipy(OH)O)Cl]$ (**2**) and $[(\eta^6\text{-tha})Ru(bipy(OH)O)(9\text{-EtG-}N7)][PF_6]$ (**10**). The phenomenon of CH/π interactions is now well-established[48] and the interaction ranges from weak (CH$\cdots\pi$ center 2.6−3.0 Å) to very strong (CH$\cdots\pi$ center <2.6 Å).[49] Such interactions can play an important role in protein stability,[48] and in recognition processes. The CH$\cdots\pi$ interactions observed for complex **1** (2.7 and 2.8 Å), where the chelating ligand is bipy (Figure 2A), are stronger (0.1 Å shorter in each case) than in complex **2** (2.8 and 2.9 Å) where the chelating ligand is bipy(OH)O (Figure 2B). This can be attributed to the greater delocalization of the π-electrons in bipy(OH)O through two possible tautomeric forms (Figure 14).

The space-filling and capped-stick models of $[(\eta^6\text{-tha})Ru(bipy(OH)O)Cl]$ (**2**) (Figure 4B,E) show the tilting of the arene toward the chelating ligand in the crystal structure,

(42) Liu, H. K.; Berners-Price, S. J.; Wang, F. Y.; Parkinson, J. A.; Xu, J. J.; Bella, J.; Sadler, P. J. *Angew. Chem., Int. Ed.* **2006**, *45*, 8153–8156.
(43) Nakamaru, K. *Bull. Chem. Soc. Jpn.* **1982**, *55*, 2697–2705.
(44) Rebek, J., Jr.; Costello, T. *Heterocycles* **1984**, *22*, 2191–2194.
(45) Rebek, J., Jr.; Trend, J. E. *J. Am. Chem. Soc.* **1978**, *100*, 4315–4316.
(46) Rebek, J., Jr.; Costello, T.; Wattley, R. V. *Tetrahedron Lett.* **1980**, *21*, 2379–2380.
(47) Rebek, J., Jr.; Costello, T.; Wattley, R. *J. Am. Chem. Soc.* **1985**, *107*, 7487–93.
(48) Brandl, M.; Weiss, M. S.; Jabs, A.; Suhnel, J.; Hilgenfeld, R. *J. Mol. Biol.* **2001**, *307*, 357–377.
(49) Bogdanovic, G. A.; Spasojevic-de Bire, A.; Zaric, S. D. *Eur. J. Inorg. Chem.* **2002**, 1599–1602.

possibly due to an intramolecular CH/π interaction[48−52] between CH protons from the outer noncoordinated ring of tha and the centers of the pyridine rings of the chelating ligand. In such interactions, the hydrogen atoms tend to lie above the centers of the aromatic rings.[51] In the previously reported crystal structure of [(η^6-tha)Ru(en)Cl][PF_6],[11] the tricyclic ring system of tha is nearly flat and the outer ring of the arene is slightly bent away from the Cl ligand. The close contact between two oxygens (O82 and O52) in the crystal structure of complex **2** suggests formation of a strong symmetrical O···H···O hydrogen bond, as observed previously in [Ni(Hdmg)]$_2$ (Hdmg = dimethylglyoxime)[53] and [Ru(bipy)$_2$(bipy(OH)O)]$^+$.[13] In the crystal structure of [(η^6-ind)Ru(bipy(OH)$_2$)Cl][PF_6] (**8**), where the chelating ligand is bipy(OH)$_2$, the distance between the two oxygens (O5A and O8A) is significantly longer than that observed in the crystal structures of [(η^6-tha)Ru(bipy(OH)O)Cl] (**2**), [(η^6-tha)Ru(bipy(OH)O)(9-EtG-*N7*)][PF_6] (**10**) and [(η^6-thn)Ru-(bipy(OH)O)(N-MeIm)][PF_6] (**11**), where the chelating ligands are in the deprotonated, bipy(OH)O form.

Intramolecular $\pi-\pi$ arene-nucleobase stacking, observed previously in [(η^6-tha)Ru(en)(9-EtG-*N7*)][PF_6]$_2$,[11] is not present in the crystal structure of complex **10**. The space-filling and capped-stick models of **10** (Figure 4C,F) clearly show that intramolecular CH/π interactions between protons from the outer ring of tha and the centers of the π-system of the chelating ligand (distances 2.8 and 3.0 Å), are present for the 9-EtG adduct as they are for the chlorido adduct (complex **2**).

Very stable H-bonding within the bipy(OH)O ligand gives rise to a large downfield shift of the resonance for the H-bonded proton ($\delta\sim18$). "Soft" and "borderline" metal ions usually prefer coordination via nitrogens of the heterocycle rather than via oxygens.[54] If the bipy(OH)O ligand was N,O-chelated instead of N,N-chelated, the resonance from the proton involved in the O−H···N hydrogen-bond would be expected to appear at $\delta\sim15$,[55−57] as observed in the ^{1}H NMR spectrum of 2,2′-bypyridine-3,3′-diol itself, where both hydrogens form O−H···N hydrogen bonds. The absence of a resonance with this chemical shift, suggests that N,N-chelation is more favorable than N,O-chelation for deprotonated bipy(OH)O. The presence of the strong O−H···O intramolecular hydrogen bond stabilizes the negative charge on the oxygen of bipy(OH)O and prevents further deprotonation/protonation within the pH range studied by NMR (2−10). It has been found previously for [Ru(bipy)$_2$(bipy(OH)O)]$^+$ that pH values of ≤ ca. 0.4 are required for protonation and of ca. 13.6 for deprotonation.[13]

Aqueous Solution Chemistry. Complexes **4**, **7**, **8** and **13**−**16** undergo relatively fast hydrolysis with half-lives of the order of minutes at 310 K (Table 3). The reported half-lives for aquation of the chlorido ethylenediamine Ru^{II} arene complexes, [(η^6-dha)Ru(en)Cl][PF_6], [(η^6-tha)Ru(en)Cl][PF_6] and [(η^6-bip)Ru(en)Cl][PF_6],[58] are 1.4−8.8 times shorter than those of complexes mentioned above, under comparable conditions. The presence of bipy as a π-acceptor in [(η^6-arene)Ru(bipy)Cl]Cl complexes where arene = benzene, *p*-cymene and hexamethylbenzene, has been reported to decrease the rate of hydrolysis by 2 orders of magnitude compared to analogues in which bipy is replaced with two aqua ligands.[59] The π-acceptor ligand bipy withdraws electron density from Ru and increases the positive charge on the metal, making it less favorable for Cl^- to leave, slowing down the hydrolysis.

For complexes which contain bip as the arene (**7** and **15**), loss of the arene is observed in aqueous solution (33% and 46%, after 24 h for complexes **7** and **15**, respectively). The same arene loss was previously observed for Ru^{II} bip complexes containing phenylazo-pyridines as π-acceptor ligands (22−50% loss of bip after 24 h in aqueous solution).[60] No arene loss was observed for the other arene complexes. Biphenyl has a high aromaticity, and competes as a π-acceptor[61] with the π-acceptor chelating ligands (bipy(OH)O and bipy in complexes **7** and **15**, respectively) for electron density. This leads to a weakening of the Ru-arene bonds and loss of bip, which is not the case for the other arenes. In **7**, the hydroxyl substituents on the chelating ligand are electron donors,[62] and the chelating ligand can exist in two tautomeric forms (Figure 14) one of which places a negative charge on the nitrogen atom. These features could make bipy(OH)O a weaker π-acceptor than bipy and stabilize the Ru^{II}-arene bonds by π-back-donation. As in both complexes (**7** and **15**) arene loss was observed, there seems to be no significant difference in the π-acceptor abilities of bipy and bipy(OH)O. Attempts to detect arene loss from the *p*-terp complex (**6**) were hampered by its very low solubility. Substituents on bipy have no significant influence on the rates of hydrolysis which suggests that their electronic effects on the metal are small, consistent with the DFT calculations.

Interactions with 9-EtG. DNA is a potential target for transition metal anticancer complexes.[63] We studied reactions of the complexes with 9-EtG as a model nucleobase. Ru^{II} complexes [(η^6-tha)Ru(bipy)Cl][PF_6] (**1**), [(η^6-tha)Ru(bipy(OH)O)Cl] (**2**) and [(η^6-bz)Ru(bipy(OH)O)Cl] (**5**) react relatively rapidly with *N7* of 9-EtG (90%, 98% and 100%

(50) Hunter, C. A.; Lawson, K. R.; Perkins, J.; Urch, C. J. *J. Chem. Soc., Perkin Trans. 2* **2001**, 651–669.
(51) Takahashi, O.; Kohno, Y.; Iwasaki, S.; Saito, K.; Iwaoka, M.; Tomoda, S.; Umezawa, Y.; Tsuboyama, S.; Nishio, M. *Bull. Chem. Soc. Jpn.* **2001**, *74*, 2421–2430.
(52) Janiak, C. *Dalton* **2000**, 3885–3896.
(53) Chakravorty, A. *Coord. Chem. Rev.* **1974**, *13*, 1–46.
(54) Hancock, R. D.; Martell, A. E. *Chem. Rev.* **1989**, *89*, 1875–914.
(55) Holligan, B. M.; Jeffery, J. C.; Norgett, M. K.; Schatz, E.; Ward, M. D. *J. Chem. Soc., Dalton Trans.* **1992**, 3345–3351.
(56) Holligan, B. M.; Jeffery, J. C.; Ward, M. D. *J. Chem. Soc., Dalton Trans.* **1992**, 3337–3344.
(57) Jeffery, J. C.; Schatz, E.; Ward, M. D. *J. Chem. Soc., Dalton Trans.* **1992**, 1921–1927.
(58) Wang, F.; Chen, H.; Parsons, S.; Oswald, I. D. H.; Davidson, J. E.; Sadler, P. J. *Chem.−Eur. J.* **2003**, *9*, 5810–5820.
(59) Dadci, L.; Elias, H.; Frey, U.; Hoernig, A.; Koelle, U.; Merbach, A. E.; Paulus, H.; Schneider, J. S. *Inorg. Chem.* **1995**, *34*, 306–315.
(60) Dougan, S. J.; Melchart, M.; Habtemariam, A.; Parsons, S.; Sadler, P. J. *Inorg. Chem.* **2007**, *46*, 10882–10894.
(61) Koefod, R. S.; Mann, K. R. *J. Am. Chem. Soc.* **1990**, *112*, 7287–7293.
(62) Kunkely, H.; Vogler, A. *Inorg. Chim. Acta* **2003**, *343*, 357–360.
(63) Zhang, C. X.; Lippard, S. J. *Curr. Opin. Chem. Biol.* **2003**, *7*, 481–489.

of binding of **1**, **2** and **5**, respectively, after 2 h in water at 310 K). 9-EtG binds to a greater extent to complexes **2** and **5** containing bipy(OH)O than to complex **1** containing bipy. In all three 9-EtG adducts (complexes **9**, **10** and **12**), the ^{1}H NMR peaks corresponding to H8 are shifted to high field relative to free 9-EtG (making the difference of 0.35, 0.63, and 0.74 ppm for complexes **9**, **10**, and **12**, respectively). Usually, metalation at the *N7* site of purine bases produces a low field shift of the H8 resonance by about 0.3−1 ppm.[64] Previously, it was observed for ethylenediamine Ru^{II} and Os^{II} arene complexes that 9-EtG H8 peaks for bound 9-EtG are shifted to low field relative to those of free 9-EtG.[10,65] However, for 9-EtG in [(η^6-*p*-cymene)Ru(acac)(9-EtG-*N7*)]$^+$ (acac = acetylacetonate), the H8 peak is shifted to high field compared to the free model nucleobase.[66] The similar H8 chemical shift behavior of 9-EtG in complexes **9**, **10** and **12** might result from the shielding of H8 by one of the pyridine rings from the bipyridine ligands (Figure 3A; H8 = C26H).

The polarization of C−H bonds of the bipy rings of bipy(OH)O and bipy chelating ligands could lead to the formation of C−H (of chelating ligand)···O (of 9-EtG) hydrogen bonds. In the crystal structure of complex **10** (Figure 3A), a hydrogen bond was observed between C20H from bipy(OH)O and O34 from 9-EtG (2.46 Å). Such C−H···O H-bonds observed in other systems commonly have bond lengths of 2.1−2.6 Å.[67]

Computation. After the geometry optimization of [(η^6-ind)Ru(bipy(OH)$_2$)Cl][PF_6] (**8**), [(η^6-ind)Ru(bipy-(Me)$_2$)Cl][PF_6] (**13**) and [(η^6-ind)Ru(bipy)Cl][PF_6] (**16**, Figure 9), VDD charges on Ru showed no significant differences among complexes (with values of +0.268 au for complexes **8** and **13** and +0.270 au for complex **16**). Therefore, substituents on bipy have no significant effect on the charge on the metal, consistent with the finding that their hydrolysis rates are similar (Table 3). Deprotonation of bipy(OH)$_2$ and chelation as bipy(OH)O is expected to reduce the positive charge on Ru^{II} since electron density from the oxygen (O^-) of one pyridine ring can be transferred onto the nitrogen of the other pyridine ring (Figure 14). However, because the H-bonded proton stabilizes the tautomer in which the negative charge is localized on the oxygen atom, this effect is weak,[13,68] as indicated by the VDD charge on Ru in deprotonated complex **8** [(η^6-ind)Ru(bipy(OH)O)Cl] of +0.271 au, similar to the charges for **8**, **13** and **16**.

The total bonding energy of tha in the optimized structure of [(η^6-tha)Ru(bipy(OH)O)(9-EtG-*N7*)]$^+$ (**10**), where the arene is interacting with the chelating ligand through the intramolecular CH/π interaction (Figure 10B), is 7.5 kJ/mol lower than the total bonding energy of tha in the optimized structure of modified complex **10**, in which there is an arene/9-EtG intramolecular $\pi-\pi$ interaction (Figure 10A). This result shows that the $\pi-\pi$ interaction between the arene and 9-EtG observed[11] for [(η^6-bip)Ru(en)(9-EtG-*N7*)][PF_6]$_2$, which might play a role in stabilizing DNA adducts, is less favored compared to CH/π interactions in complex **10**. This may lead to less stable DNA adducts.

Cancer Cell Growth Inhibition. Complex **1**, containing tha as the arene and bipy as the chelating ligand, showed no activity in either the A2780 human ovarian or A549 human lung cancer cell lines, consistent with our previous report of the inactivity of bipy/ind and bipy/bip complexes.[10] Complexes containing bipy(OH)O as the chelating ligand show a dramatic increase in cytotoxicity compared to their bipy analogues (Table 4).[10] The higher IC_{50} (lower cytotoxicity) value for [(η^6-bip)RuCl(bipy(OH)O)] (complex **7**; 40 μM in A2780 cells), compared to most of the other complexes containing bipy(OH)O, may be related to the facile loss of arene in this case. The low solubility of [(η^6-*p*-terp)Ru(bipy(OH)O)Cl] (**6**) hindered studies of arene loss during aquation of this complex. No arene loss was observed in other complexes studied here.

DNA Binding. Complexes **16** and **8** bind to DNA to a relatively small extent. (~10 to ~40% after 48 h). CD spectra showed (Figure 11) that the binding of **16** results in conformational alterations in double-helical DNA of a nondenaturational character, similar to those induced in DNA by conventional antitumor cisplatin. In contrast, the binding of **8** results in conformational alterations in DNA of a denaturational character, similar to those induced in DNA by clinically ineffective transplatin. In addition, complex **16** interacts with DNA via both covalent and noncovalent interactions. The melting behavior of DNA was affected by **16** and **8** only negligibly (t_m was changed by less than 1 K) and the ability of complex **16** to displace DNA intercalator EtBr from CT DNA was considerably greater than that of complex **8** (Figure 12). These results do not explain the dramatic difference in anticancer activity of **8** (Table 4; IC_{50} = 18 and 39 μM, against A2780 and A549 cells, respectively) and **16** (IC_{50} > 100 μM against A2780 cells),[10] and so it seems likely that DNA is not a major target for these complexes.

Differences in structure and overall charge of complexes **8** and **16** might lead to differences in their activity. Further studies are needed to further explore potential cellular targets, which might include key cellular signaling pathways. Recently, a series of neutral cyclopentadienyl ruthenium complexes has been designed which mimic the structural features of small organic molecule inhibitors and target the ATP-binding site of protein kinases,[69] including phosphatidyl-inositol-3-kinase (PI3K) which is involved in cancer cell survival. H-bonding is important in such inhibition.[70] Complex **8** has a potential to form H-bonds and may be a more effective enzyme inhibitor than complex **16**.

(64) Scheller, K. H.; Scheller-Krattiger, V.; Martin, R. B. *J. Am. Chem. Soc.* **1981**, *103*, 6833–6839.
(65) Peacock Anna, F. A.; Habtemariam, A.; Fernandez, R.; Walland, V.; Fabbiani Francesca, P. A.; Parsons, S.; Aird Rhona, E.; Jodrell Duncan, I.; Sadler Peter, J. *J. Am. Chem. Soc.* **2006**, *128*, 1739–1748.
(66) Fernandez, R.; Melchart, M.; Habtemariam, A.; Parsons, S.; Sadler, P. J. *Chem.−Eur. J.* **2004**, *10*, 5173–5179.
(67) Steiner, T. *Chem. Comm.* **1997**, 727–734.
(68) Himeda, Y.; Onozawa-Komatsuzaki, N.; Sugihara, H.; Arakawa, H.; Kasuga, K. *Stud. Surf. Sci. Catal.* **2004**, *153*, 263–266.
(69) Bregman, H.; Williams, D. S.; Atilla, G. E.; Carroll, P. J.; Meggers, E. *J. Am. Chem. Soc.* **2004**, *126*, 13594–13595.
(70) Xie, P.; Williams, D. S.; Atilla-Gokcumen, G. E.; Milk, L.; Xiao, M.; Smalley, K. S. M.; Herlyn, M.; Meggers, E.; Marmorstein, R. *ACS Chem. Biol.* **2008**, *3*, 305–316.

Conclusion

Here, we have shown for the first time that half-sandwich Ru^{II} arene complexes containing deprotonated 2,2′-bipyridine-3,3′-diol (bipy(OH)O) as the chelating ligand can exhibit significant cytotoxic activity toward cancer cells, in contrast to analogous complexes containing bipyridine or bipyridine with 4,4′-substituents such as Me. X-ray crystal structures and ^{1}H NMR spectroscopy have shown that deprotonated bipy$(OH)_2$ (bipy (OH)O) can form a strong intraligand H-bonding system which enforces planarity on bipy(OH)O. We have shown that strong binding to 9-EtG can occur for complexes containing bipy(OH)O as well as for those containing bipy. An interesting feature of the structures of complexes with tha as arene is the presence of arene CH$\cdots\pi$ (bipy(OH)O and bipy) interactions. With the use of DFT calculations, these interactions were found to be more stable compared to $\pi-\pi$ interactions between the arene and 9-EtG; the latter are known to stabilize DNA adducts. This work illustrates that subtle features in organometallic complexes can exert major effects on biological activity. However, DNA binding studies suggest that neither bipy nor bipy(OH)O complexes bind strongly to DNA, suggesting that DNA is not the major target for these complexes. Further studies are needed to identify potential targets.

Acknowledgment. We thank Oncosence Ltd, ORSAS and University of Edinburgh for financial support for T.B., and Emily Jones and Daniel Simpson (Oncosense Ltd) for cytotoxicity tests. This research was supported by the Ministry of Education of the CR (MSMT LC06030, 6198959216, ME08017, OC08003), the Academy of Sciences of the Czech Republic (Grants 1QS500040581, KAN200200651, AV0Z50040507 and AV0Z50040702), the Grant Agency of the Academy or Sciences of the CR (IAA400040803) and the Grant Agency of the Ministry of Health of the CR (NR8562-4/2005). J.K. is the international research scholar of the Howard Hughes Medical Institute. The authors also acknowledge that their participation in the EU COST Action D39 enabled them to exchange regularly the most recent ideas in the field of anticancer metallodrugs with several European colleagues.

Supporting Information Available: H-Bonding interactions for complexes **1**·H_2O, **2**, **8**·CH_3O, **10**·CH_3OH and **11** (Table S1) and circular dichroism (CD) spectra of calf thymus DNA modified by complex **16** (Figure S1). This material is available free of charge via the Internet at http://pubs.acs.org.

IC801361M